

**A PERFECTLY MATCHED LAYER (PML)
FOR ELECTROACOUSTIC WAVES IN PIEZOELECTRIC
MATERIALS USING FDTD**

**PERFECTLY MATCHED LAYER (PML) FOR
ELECTROACOUSTIC WAVES IN PIEZOELECTRIC
MATERIALS USING FDTD**

By:

ARTHUR O. MONTAZERI, B.ENG.

A Thesis

Submitted to the School of Graduate Studies

In Partial Fulfillment of the Requirements

for the Degree

Master of Applied Science

September 2010

McMaster University

© Copyright by Arthur Montazeri, August 2010

MASTER OF APPLIED SCIENCE (2010)
(Electrical Engineering)

McMaster University
Hamilton, Ontario

TITLE: A PML for Electroacoustic Waves in Piezoelectric Materials using FDTD

AUTHOR: Arthur O. Montazeri, B.Eng. (McMaster University)

SUPERVISORS: Professor M. Bakr, Professor Y. Haddara

NUMBER OF PAGES: viii, 83

Abstract

An improved Perfectly Matched Layer (PML) boundary condition is introduced that addresses the previously reported instabilities. A PML for acoustic waves is derived by closely following Bérenger's derivation of a PML for electromagnetic waves. A new matching condition is developed to relate the velocity and stress loss-coefficients similar to the matching condition defined for electromagnetic waves.

Whereas, the spatial and temporal derivatives are related by simple scalars in Maxwell's equations, elastodynamic equations describing waves in piezoelectric materials require the use of tensor quantities whose general forms are material dependent.

In practice, SAW generation is often also accompanied by some small creation of BAWs, which act as parasitic waves. It is thus desired to remove the reflection of these waves from the bottom, in both physical SAW devices and in modeling.

Acknowledgements

I would like to thank Dr. M. Bakr, for his unwavering support, supervision, and presence, throughout this study. I would also like to thank my co-supervisor Dr. Y. Haddara.

Lastly, I am greatly indebted to my late father, who has been, and will always be, a source of inspiration in my life. This work is dedicated to his memory.

Contents

1.	INTRODUCTION TO SURFACE ACOUSTIC WAVES AND DEVICES	1
1.1	INTRODUCTION TO SURFACE ACOUSTIC WAVES	1
1.2	SAW DEVICES ON PIEZOELECTRIC MATERIALS AND THEIR APPLICATION IN ELECTRONICS	1
1.3	TYPES OF WAVES IN SOLIDS	2
1.3.1	SAWs	3
1.3.2	Bulk Acoustic Waves	3
1.3.2	Pseudo-SAWs (PSAWs)	3
1.4	ADVANTAGES OF SAW DEVICES OVER ELECTRONIC COMPONENTS	4
1.5	PIEZOELECTRIC-BASED SAWs	4
1.5.1	Piezoelectric Materials	4
1.5.1.1	Piezoelectric Efficiency, and Materials Considerations	4
1.6	THE NEED FOR MODELLING AND SAW SIMULATORS	5
1.6.1	Available Models	5
1.7	THE GOALS OF THIS RESEARCH AND THE ORGANIZATION OF THIS THESIS	6
1.7.1	Research Motivation and Objectives	6
1.7.2	Thesis Organization	7
2.	MATERIALS REVIEW, PHYSICS OF PIEZOELECTRICITY, AND SAW GENERATION	8
2.1	STRESS AND STRAINS IN SOLIDS	8
2.2	THE WAVE EQUATION IN SOLIDS	13
2.3	PIEZOELECTRICITY	17
2.4	EQUATIONS GOVERNING PIEZOELECTRICITY	17
2.5	CRYSTAL CLASSIFICATION SYSTEMS	21
2.6	SOLUTIONS OF THE ELECTROACOUSTIC WAVE EQUATIONS	22
2.7	QUASISTATIC ASSUMPTION	23
2.8	SOLUTIONS OF THE ELASTODYNAMIC EQUATIONS	24
2.9	CHRISTOFFEL'S EQUATION AND SLOWNESS CURVES	25
2.10	WAVE EQUATION IN SOLIDS	25
3.	SAW DEVICES AND DEVICE MODELING	31
3.1	ANATOMY OF A TYPICAL SAW DEVICE	31
3.2	REFLECTOR-BASED SAW APPLICATIONS	32
3.3	FREQUENCY OF OPERATION OF SAW DEVICES	35
3.4	DOMAIN OF SIMULATION	36
3.5	REVIEW OF AVAILABLE METHODS AND SIMULATION TECHNIQUES	37
3.5.1	Rigorous vs. Phenomenological Techniques	38
3.5.2	Development of Approximate Field-Theoretical Formulations	38
3.6	BOUNDARY CONDITION CONSIDERATIONS	39
3.7	CURRENT STATE OF WORK ON SOLUTIONS OF NUMERICAL FIELD-EQUATIONS	41
3.8	FINITE DIFFERENCE METHOD (FDTD)	42

3.9	THE FDTD SIMULATOR	46
4.	ABSORBING BOUNDARY CONDITIONS	49
4.1	REVIEW OF THE EXISTING BOUNDARY CONDITIONS FOR ACOUSTIC WAVES	49
4.2	REVIEW OF THE ABSORBING BOUNDARY CONDITIONS FOR ELECTROMAGNETIC WAVES	50
4.3	PML FOR ELASTODYNAMIC WAVES	52
	4.3.1 A Review of Elastodynamic Wave Scattering from Boundaries	52
4.4	DERIVATION OF THE ELASTODYNAMIC PML BASED ON BÉRENGER'S APPROACH	56
4.5.	APPLYING THE MATCHING CONDITION TO DERIVE THE PML TIME UPDATE EQUATIONS	60
4.6	SIMULATION RESULTS OF THE IMPLEMENTED PML	65
	4.6.1. Domain Definition and Simulation Parameters	65
	4.6.2. Results	67
5.	CONCLUSIONS	74
	REFERENCES	75
	APPENDIX	79

List of Figures

Figure 1: Compressional Stress	8
Figure 2: Shear Force Acting on Area A	9
Figure 3: Particle Displacement	14
Figure 4: A Sample Slowness Curve for a Cubic Crystal (GaAs)	30
Figure 5: SAW generation and Detection using IDTs	32
Figure 6: IDTs on a SAW Device	33
Figure 7: SAW Structure Characteristic Lengths	34
Figure 8: Domain Representing One IDT Finger on the Sagittal Plane	37
Figure 9: Yee's Leapfrog Algorithm	43
Figure 10: Staggered Stress and Velocity Field Values Based on Yee's- Approach for Simulation of Electromagnetic Waves	45
Figure 11: Block-Diagram of the Implemented SAW FDTD Simulator in C++	47
Figure 12: Boundary Scattering of Coupled Elastodynamics Waves	53
Figure 13: Comparison of the Normalized T_{xx} Field Component for an Unbounded Medium and the PML	67
Figure 14: Excitation near the PML	69
Figure 15: SAW Excitation under Metallic IDT	70
Figure 16: Absorption of the Parasitic Waves by the PML	72

Chapter 1: Introduction to Surface Acoustic Waves and Devices

1.1 Introduction to Surface Acoustic Waves

Surface Acoustic Waves (SAWs) in solids, are quite commonplace in nature. SAWs are mechanical waves that travel in a superficial region of a solid [1]. In a true SAW (also referred to as a Rayleigh wave,) particles near the surface have an elliptical motion that stays close to the free surface of the solid. The motion of this wave, as we will see later, resembles a rolling water wave.

Originally, this wave was discovered by lord Rayleigh in mid 19th century [2]. Rayleigh waves are produced during earthquakes, explosions, or upon impact on hard surfaces, such as the action of a hammer on a concrete slab. They can also be produced on very small scales on solid crystals. This latter is the basis of their application in electronics, examined herein.

1.2 SAW Devices on Piezoelectric Materials and Their Application in Electronics

The application of SAWs in electronics started when they could be generated by applying an electric signal to thin metallic films deposited on a piezoelectric crystal. These materials are capable of converting electric excitations into mechanical (acoustic) waves and vice versa [3].

In 1969, Tancrell et al. showed the first results of a SAW device on a lithium niobate substrate, which is a piezoelectric material. This was the pioneering work resulting in the modern SAW devices. The breakthrough step was the use of a piezoelectric material.

The first demonstration of piezoelectric materials dates back to 1880, by P. and J. Curie [4]. Curies discovered that charge accumulates on the surface of certain crystals, when they are subjected to mechanical stress. However, the inverse piezoelectric effect (that an electric voltage applied to the surface of these materials, generates internal stresses) was not predicted by the Curies [5]. This inverse effect was first mathematically predicted by Gabriel Lippmann in 1881 [6]. The Curies quickly confirmed the proposed inverse effect, and proceeded to obtain quantitative measures of this reversible electro-acoustic effect in piezoelectric crystals. In fact, it is now known that the direct piezoelectric effect is always accompanied by the inverse piezoelectric effect [3].

1.3 Types of Waves in Solids

The waves in solids can be categorized based on the position of the travelling wave and the mechanism of the wave propagation. The waves are either localized in a small region near the surface of the material, in which case they are labelled as surface waves, or they propagate into the medium, in which case they are called bulk acoustic waves. The other classification is based on the particle displacement pattern with respect to the direction of propagation. If the particle motion is in the direction of the wave

propagation, the wave is of longitudinal or compressional type. Waves in which the direction of particle motion is perpendicular to the propagation direction are called transverse or shear.

This research mainly focuses on SAWs, but it is worth mentioning that SAWs are but a class of possible waves that can exist inside solids. Other wave types have also found practical applications in device design.

1.3.1 SAWs

These are surface waves with a localized perturbation pattern near the free surface of the substrate in which they propagate.

1.3.2 Bulk Acoustic Waves (BAWs)

The motion of bulk waves, as their name suggests, is not restricted to a thin region on the surface of the material, but they radiate into the substrate. It is expected then, that the response of a device built based on BAWs depend on the thickness of the substrate.

1.3.3 Pseudo-SAWs (PSAWs)

Pseudo-SAW devices combine the characteristics of both surface and bulk acoustic waves. These waves have more than one component: one which travels near the surface, as well as a component that radiates into the substrate.

1.4 Advantages of SAW Devices over Electronic Components

SAW devices have several qualities that make them attractive for electronics. A simple SAW device can perform complex functions such as band-pass filtering, etc. that would otherwise require a great number of electronic components. This makes SAW devices very compact and suitable for these signal processing tasks in microelectronic devices such as mobile phones. SAW devices are also quite energy efficient and low loss, thanks to the localization of energy and low dissipation. Their cost of fabrication is comparable to typical semiconductors, and in fact optical photolithography which is used for semiconductor fabrication is usually also used for SAWs. This keeps SAW device production cost effective and enables their mass production in a parallel method. As well, micro-acoustic devices including SAW devices, have higher quality factors compared to electromagnetic components, even in the GHz frequencies.

1.5 Piezoelectric-Based SAWs

1.5.1 Piezoelectric Materials

Piezoelectric materials occur naturally, and examples include: quartz, topaz, bone, and sugar crystals. Man-made piezoelectric materials have also been produced which generally exhibit better piezoelectric efficiencies. Lithium niobate, and barium titanate are examples of these synthetic materials.

1.5.1.1 Piezoelectric Efficiency, and Materials Considerations

Even though naturally occurring piezoelectric materials exist, their efficiency in converting electrical to acoustic energy, and vice versa, is inferior to some of the man-made materials. Hence, a great deal of effort has been made to create better and more efficient piezoelectric materials.

1.6 The Need for Modelling and SAW Simulators

Fabrication of SAW devices requires design, materials, clean-rooms, technicians, and is a time consuming process. As SAW device designs become more complicated, fabrication process of devices becomes even more time consuming and consequently more expensive. These factors give reason for developing accurate models that reduce design and production errors, and significantly cut down costs.

This makes accurate simulators, which can predict device response before the onset of fabrication, an extremely powerful tool for the industry.

Additionally, simulations reduce the cost of experimenting with various design parameters such as: IDT geometry, substrate materials, device thicknesses, metallic film thickness, and so forth. Such a tool enables a more thorough computer-aided requirement analysis, and higher quality devices.

1.6.1 Available Models

Various models have been proposed and implemented for SAW devices, and other types of acoustic waves. These models can be divided into two groups: physics-based models, and phenomenological models. The former, namely, physics-based models use various techniques to solve the differential equations, which governing the generation of waves in piezoelectric materials. In comparison, phenomenological models, cannot start directly from the design parameters and predict the output response. Their use requires supplying of a certain set of parameters. These parameters can either be obtained from measurements taken experimentally, or from physics-based simulators. These two models are thus often complementary than substitutive. We will examine some of these models in more detail in Chapter 3.

1.7 The Goals of this research and the Organization of this Thesis

1.7.1 Research Motivation and Objectives

In this research, a time-domain physics-based simulator of SAWs is developed. An improved perfectly matched layer (PML) is introduced for defining the computational domain that does not experience the previously reported instability issues [10]. The simulator is implemented in C++ and the PML is employed to simulate an unbounded medium. This work is discussed in detail in Chapter 4.

In numerical modeling, requirements of certain problems will require the simulation of an unbounded space. Computationally this has to be in a finite domain. For instance, in antenna simulation, this problem is often faced, where the antenna features

are to be studied in an unbounded, unobstructed surrounding. As we will see, absorbing boundary conditions (ABCs) allow the simulation of such an unbounded medium, in a finite, and often relatively small computational domain. Absorbing boundary conditions are general class of boundary conditions, used to simulate the reflectionless propagation of waves.

1.7.2 Thesis Organization

This document is organized into 5 chapters as follows:

Chapter 2 provides a mathematical introduction to elastodynamic waves on piezoelectric materials, and lays the foundation for a physics-based model implemented in this work.

Chapter 3 discusses the existing physics-based models for the simulation of SAWs, and compares the frequency domain and time domain techniques, their advantages and shortcomings.

Chapter 4 discusses the developed method in this research in detail, along with the results, and a discussion on the findings.

Chapter 5 gives the conclusion of the work and findings

Chapter 2: Materials Review, Physics of Piezoelectricity, and SAW generation

2.1 Stress and Strains in Solids

Let us first consider the relation between stress T and strain S for small static deformations in a solid. Stress is defined as the force per unit area of the solid onto which a force is applied and has units of $[\text{N}/\text{m}^2]$, with the force being measured in units of $[\text{N}]$. This is defined as:

$$T = \frac{F}{A} \quad (1)$$

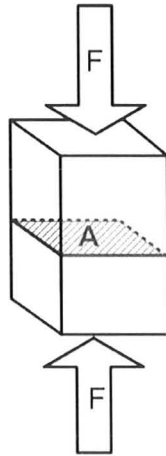


Figure 1 Compressional Stress

Strain is defined as a dimensionless quantity:

$$S = \frac{\Delta}{L} \quad (2)$$

where Δ is the lineal deformation expressed as a percentage of L .

The existence of stresses and strains in solids can be of compressional or shear type. The former are those where the applied force is normal to the area upon which the force acts (Figure 1.) Shear forces are referred to those, which act in the plane of A as opposed to normal to it (Figure 2.) Plane A , in equation (1) refers to the area A along with a direction which is taken as the surface normal vector.

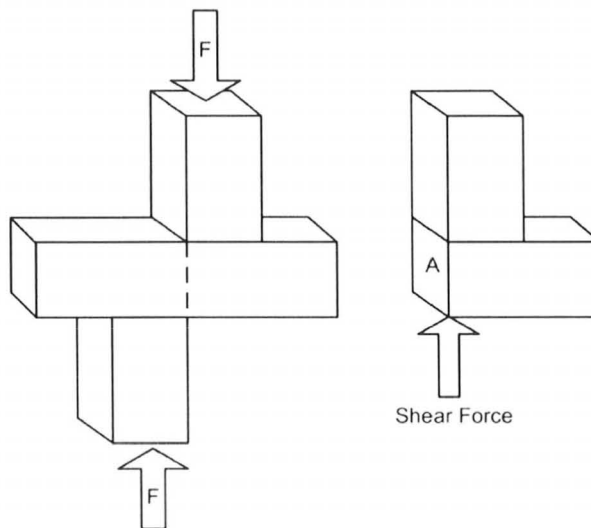


Figure 2 Shear Force Acting on Area A

In its simplest form, Hooke's law relates compressional stress and strain:

$$T = cS. \quad (3)$$

where c is the stiffness, generally referred to as the Young's modulus of the material. As stated however, equation (3) will only apply to the longitudinal stress-strain types shown in Figure 1. In order to generalize this to include all possible components of the stress field (defined shortly below,) it is necessary to use tensor quantities:

$$(T) = (c):(S). \quad (4)$$

Summarized by the indexed tensor equation [5].

$$T_{ij} = c_{ijkl}S_{kl}, \quad (5)$$

where $i, j, k, l = x, y, z$. In this notation an implicit summation over the repeated subscripts k, l is made:

$$T_{ij} = \sum_{k,l=1}^3 c_{ijkl}S_{kl}, \quad (6)$$

Now for example the T_{xx} component of the stress is given by:

$$\begin{aligned} T_{xx} = & c_{xxxx}S_{xx} + c_{xxyy}S_{yy} + c_{xxzz}S_{zz} \\ & + c_{xxyx}S_{yx} + c_{xyyy}S_{yy} + c_{xyyz}S_{yz} \end{aligned} \quad (7)$$

$$+c_{xxzx}S_{zx} + c_{xxzy}S_{zy} + c_{xxzz}S_{zz}.$$

Since equation (5) is in fact 9 equations for all combinations of i and j , the total number of stiffness coefficients is 81. However, not all these equations are independent, and in fact it can be shown that [5]:

$$c_{ijkl} = c_{jikl} = c_{ijlk} = c_{jilk}, \quad (8)$$

reducing the total number of equations to 36.

In this generalized form, the force components can take arbitrary alignment with the area upon which they act. This is expressed as:

$$T_{jk} = \frac{F_j}{A_k}, \quad (9)$$

where j denotes the direction of the force application, and k denotes the plane of action, defined as the surface normal to plane A . (c) in equation (4) is a fourth rank tensor, and is used to relate quantities in two different coordinate systems such as for instance, T_{xy} to S_{yz} [5].

For simplicity, when symmetry allows, tensor equations such as equation (3) are converted into matrix equations. As a result, the following abbreviations will henceforth be used:

$$T_{xx}=T_1, T_{yy}=T_2, T_{zz}=T_3, \quad (10)$$

$$T_{zy} = T_{yz} = T_4, T_{zx} = T_{xz} = T_5, T_{xy} = T_{yx} = T_6$$

In referring to \mathbf{T} hereon, this abbreviated notation will be implied, that is:

$$\mathbf{T} = \begin{bmatrix} T_1 \\ T_2 \\ T_3 \\ T_4 \\ T_5 \\ T_6 \end{bmatrix}. \quad (11)$$

Using the abbreviated notation, stress-strain relationship can be written as:

$$T_I = c_{IJ}S_J, \quad (12)$$

with I and J now varying from 1 to 6. Furthermore, the 6×6 compliance (or its inverse which is stiffness) matrix will now have only 21 unique components, as all the unique coefficients can be expressed as a 6×6 triangular matrix. In other words, the stiffness matrix is symmetric for all crystal classes, even those with the least degree of symmetry. For crystal classes with higher order of symmetry, the number of independent elements is less.

There exists an alternative representation of equation (5), which expresses strains as a linear combination of stresses.

$$S_{ij} = s_{ijkl}T_{kl}, \quad (13)$$

where $i, j, k, l = x, y, z$. The tensor constants s_{ijkl} relating these two in this case are called the compliance coefficients. This value is in fact a measure of deformability indicating how easy or difficult it is to deform the material [5]. The larger this value is, the larger the deformation, and the softer the material is. On the other hand deformation is smaller for stiffer materials, and as a result, harder materials have lower values of s . Experimentally measured stiffness values are within 0.1×10^{10} N/m² for rubbery, flabby materials, to 10×10^{10} for single crystals and metals. The matching compliance coefficients are 1000×10^{-12} to 10×10^{-12} m²/N [5].

2.2 The Wave Equation in Solids

Let us start by differentiating equation (6) with respect to space:

$$\sum_{j=1}^3 \frac{\partial T_{ij}}{\partial x_j} = \sum_{j,k,l=1}^3 c_{ijkl} \frac{\partial S_{kl}}{\partial x_j} = \sum_{j,k,l=1}^3 c_{ijkl} \frac{\partial^2 u_k}{\partial x_j \partial x_l} \quad (14)$$

By using the following definition for strain:

$$S_{kl} = \frac{1}{2} \left(\frac{\partial u_i}{\partial x_j} + \frac{\partial u_j}{\partial x_i} \right), \quad (15)$$

where \mathbf{u} is the particle displacement field describing the vibrational motion of all particles within a given solid (Figure 3.) For instance for a particle positioned at location L , the displacement measured from the origin is:

$$\mathbf{u}(L, t) = \mathbf{l}(L, t) - L, \tag{16}$$

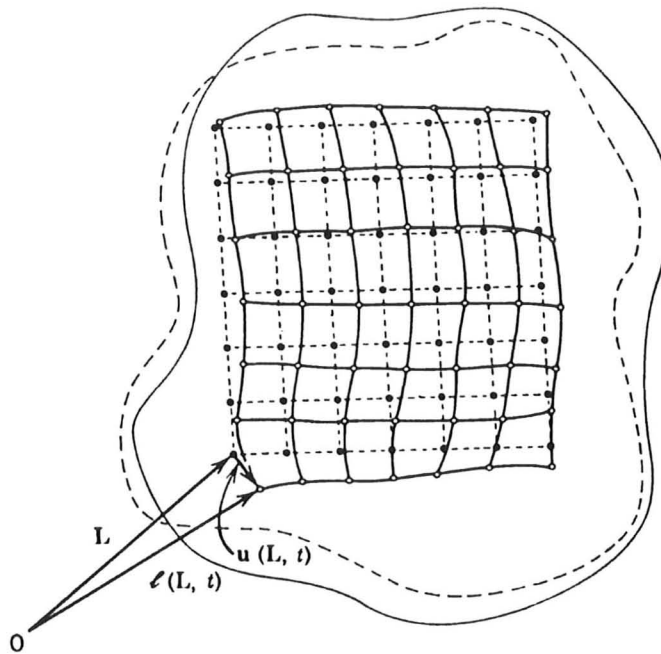


Figure 3 Particle Displacement [5]

We understand deformation, not by the displacement field given by equation (16), because translation and rotation too will have a nonzero displacement. Thus, a more robust definition of deformation or strain is needed. Equation (15), called the linearized strain displacement, corresponding to an infinitesimal displacement, resolves the ambiguity among strain, translation, and rotation.

Using the equation of motion, which is:

$$\sum_{j=1}^3 \frac{\partial \mathbf{T}_{ij}}{\partial x_j} = \rho \frac{\partial^2 \mathbf{u}_i}{\partial t^2}, \quad (17)$$

the wave equation is obtained:

$$\rho \frac{\partial^2 \mathbf{u}_i}{\partial t^2} = \sum_{j,k,l=1}^3 c_{ijkl} \frac{\partial^2 \mathbf{u}_k}{\partial x_j \partial x_l}, \quad (18)$$

with i varying from 1 to 3 representing the three coordinate axes.

The plane wave solutions of equation (18) can have the form:

$$\mathbf{u}_i(x, t) = u_0 e^{(j\omega t - kx)}. \quad (19)$$

As previously stated, this solution depends on the material choice and the direction of propagation, and both these criteria change the stiffness matrix. The stiffness matrices for all classes of materials are presented in Appendix A. Here, the wave solutions for the simple isotropic materials are given. Though the form of the wave equations holds valid for all types of materials, the solutions can look very different for materials with different crystal symmetries. For an isotropic material then:

$$\rho \frac{\partial^2 u_1}{\partial t^2} = c_{11} \frac{\partial^2 u_1}{x^2},$$

$$\rho \frac{\partial^2 u_2}{\partial t^2} = c_{44} \frac{\partial^2 u_2}{x^2}, \quad (20)$$

$$\rho \frac{\partial^2 u_3}{\partial t^2} = c_{44} \frac{\partial^2 u_3}{x^2}.$$

Which simplify to:

$$\rho \omega^2 = c_{11} k^2,$$

$$\rho \omega^2 = c_{44} k^2, \quad (21)$$

$$\rho \omega^2 = c_{44} k^2.$$

This has three acoustic wave solutions, with three (in general different) velocities, per direction of propagation. These velocities are:

$$v_1 = \sqrt{\frac{c_{11}}{\rho}},$$

$$v_2 = v_3 = \sqrt{\frac{c_{44}}{\rho}}, \quad (22)$$

where v_1 is a compressional wave, and the two other waves are shear.

2.3 Piezoelectricity

A detailed mathematical explanation of piezoelectricity is given in [5]. A brief and qualitative description of piezoelectricity can be given by a simple atomic model however. In the case of the direct piezoelectric effect, the external force, deforming the material, displaces the atoms, generating electric dipole moments inside the material. In piezoelectric materials, these electric dipoles tend to be more organized, causing polarization.

This direct effect is always a reversible phenomenon for all piezoelectric materials. That is, in the presence of an electric field, the charge separation of the atoms creates a strain in the material. This is called the inverse piezoelectric effect. Both these effects are linear, and the change in sign of the applied field is accompanied by a change in sign of the strain, and vice versa.

2.4 Equations Governing Piezoelectricity

Application of an electric field to a non-piezoelectric material results in no macroscopic mechanical effects, while an electric field creates mechanical deformations in piezoelectric materials. In reality, changes to the electrical field will give rise to mechanical deformations, and these will in turn contribute to the electric field and the process continues. Also known as the piezoelectric constitutive relations, the piezoelectric equations are written as:

$$\mathbf{D} = \boldsymbol{\epsilon}^T \cdot \mathbf{E} + \mathbf{d} : \mathbf{T}, \quad (23)$$

$$\mathbf{S} = \mathbf{d}' \cdot \mathbf{E} + \mathbf{s}^E : \mathbf{T}, \quad (24)$$

where the dot and double dot products indicate summation over single and double subscripts respectively. For instance $\boldsymbol{\epsilon}^T \cdot \mathbf{E}$ is the summation over all j when written as: $\epsilon^T_{ij} \cdot E_j$, and $\mathbf{d} : \mathbf{T}$ represents $d_{ijk} \cdot T_{jk}$ with summation over both j and k . In the above equations, \mathbf{S} is the strain, \mathbf{E} is the electric field, \mathbf{D} is electrical displacement, \mathbf{T} is the stress tensor, $\boldsymbol{\epsilon}^T$ is the 3×3 dielectric permittivity matrix measured under constant stress, and \mathbf{d} is defined as the piezoelectric strain constants matrix, whose inverse is denoted by a prime. This form of the equations is known as the strain-displacement, or the piezoelectric strain equations. Because it is common in the literature to also use piezoelectric stress-displacement relations, it is worthwhile to note that an equivalent form of equations (23) and (24) are:

$$\mathbf{D} = \boldsymbol{\epsilon}^S \cdot \mathbf{E} + \mathbf{e} : \mathbf{S}, \quad (25)$$

$$\mathbf{T} = -\mathbf{e} \cdot \mathbf{E} + \mathbf{c}^E : \mathbf{S}, \quad (26)$$

with \mathbf{e} defined as the piezoelectric displacement, and \mathbf{c}^E is the stiffness matrix.

Equations (25) and (26) are collectively referred to as the piezoelectric constitutive equations.

Maxwell's equations, together with piezoelectric constitutive relations provide the physics of propagation of acoustic waves on piezoelectric substrates. This is summarized below:

$$\nabla \times \mathbf{E} = -\frac{\partial \mathbf{B}}{\partial t} = -\mu \frac{\partial \mathbf{H}}{\partial t}, \quad (27)$$

$$\nabla \times \mathbf{H} = \frac{\partial \mathbf{D}}{\partial t} = \frac{\partial}{\partial t} (\boldsymbol{\epsilon}^T \cdot \mathbf{E} + \mathbf{d} : \mathbf{T}), \quad (28)$$

$$\nabla_s \mathbf{v} = \frac{\partial \mathbf{S}}{\partial t} = \frac{\partial}{\partial t} (\mathbf{d}' \cdot \mathbf{E} + \mathbf{s}^E : \mathbf{T}), \quad (29)$$

$$\nabla \cdot \mathbf{T} = \rho \frac{\partial \mathbf{v}}{\partial t} - \mathbf{F}. \quad (30)$$

where

\mathbf{E} is the electric field vector,

\mathbf{B} is the magnetic flux density vector,

$\boldsymbol{\epsilon}^T$ is the 3×3 electric permittivity matrix under constant stress,

μ is the permeability,

\mathbf{d} is the piezoelectric strain coefficient matrix,

\mathbf{T} is the stress vector,

\mathbf{v} is the particle velocity vector,

\mathbf{S} is the strain vector,

\mathbf{d}' is transpose of \mathbf{d} ,

\mathbf{s}^E is the 6×6 compliance coefficient matrix measures under constant electric field,

ρ is the material density,

\mathbf{F} is the body force vector,

$$(\nabla_s)' = \begin{bmatrix} \partial/\partial x & 0 & 0 & 0 & \partial/\partial z & \partial/\partial y \\ 0 & \partial/\partial y & 0 & \partial/\partial z & 0 & \partial/\partial x \\ 0 & 0 & \partial/\partial z & \partial/\partial y & \partial/\partial x & 0 \end{bmatrix}.$$

Equation (27) is just the Maxwell equation in rationalized units. The solutions which simultaneously satisfy the above equations describe the motion of waves in piezoelectric materials. In non-piezoelectric materials, the acoustic and electromagnetic solutions are completely independent of each other and are decoupled. But in piezoelectric materials, they are coupled through the piezoelectric strain equations. Equations (28) and (29) denote this tie between the strain and the electric field in piezoelectric solids. Let us examine each term in detail:

$$\nabla \times \mathbf{H} = \frac{\partial \mathbf{D}}{\partial t} = \frac{\partial}{\partial t} (\boldsymbol{\epsilon}^T \cdot \mathbf{E} + \mathbf{d} : \mathbf{T}), \quad (31)$$

$$\nabla_s \mathbf{v} = \frac{\partial \mathbf{S}}{\partial t} = \frac{\partial}{\partial t} (\mathbf{d}' \cdot \mathbf{E} + \mathbf{s}^E : \mathbf{T}). \quad (32)$$

The first terms in the parenthesis of equations (31) and (32) give respectively the electric displacement, and the strain, in response to the electric field, which are generated through the application of an external voltage. Due to this aforementioned strain, in a mechanically confined medium, stresses will develop in response to this strain. This stress now modifies the relationship between \mathbf{D} and \mathbf{E} , by contributing to the second term of equation (31) [5]. In the absence of this term, the relation between \mathbf{D} and \mathbf{E} is that of simple dielectrics.

And the reverse also holds true, that is, a strain, related to the stress through mechanical constraints, is produced in response to a stress in the medium. These two equations together, explain the relation between the stress field components T_{ij} and mechanical deformations by the strain S_{ij} .

The preceding was a brief mathematical overview of the acoustic field equations together with the electromagnetic equations. Analytical solutions for these equations are only available for the simplest crystals, and only in certain directions of propagation.

2.5 Crystal Classification Systems

Based on the arrangement of their constituent atoms, solids take on various structural systems. There is a finite number of possibilities. In fact, all anisotropic crystals can be categorized into nine classes, by specifying their stiffness matrices. In Appendix A, all these crystal classes are given. As mentioned earlier, the most number of unique stiffness constants are 21, and this corresponds to the triclinic crystal system. In the other extreme, the most symmetric materials are isotropic systems, with only 2 independent stiffness coefficients. As we will see when solving for the wave equation, and also in dealing with boundary condition, the crystal classification has a direct impact in determining the complexity of the solution.

2.6 Solutions of the Electroacoustic Wave Equations

Maxwell's equations namely equations (27) and (28), have two plane wave solutions. The acoustic waves, i.e. equations (29) and (30), have three plane wave solutions for each direction.

As it is clear from equations (28) and (29), if the material is non-piezoelectric, the acoustic and electromagnetic solutions are completely independent of each other. This is simply because the terms involving the electric field drop out of the last two equations for non-piezoelectric materials. The stress (or strain) equations, create a coupling between the five types of plane waves mentioned above [5].

Which of these solutions become coupled, depends on the materials properties, most importantly on the symmetry classification. As well, the direction of the wave

propagation changes the coupling between the waves. In certain crystals, and for specific propagation directions, waves of a pure type, without coupling to others can exist. These directions are often of practical interest for device design, and they enable the use of pure waves for the device operation. For such set ups, the presence of other modes is usually considered parasitic.

2.7 Quasistatic Assumption

In solving these equations, it is often worthwhile to consider the quasistatic assumption. It is important to realize where this assumption stems from. When solving these equations, it becomes apparent that the coupling between acoustic waves and electromagnetic waves, (even for the strongest piezoelectric materials,) is relatively small in comparison by the effects of the quasistatic electric field [5]. A quasistatic electric field is one which is non-rotational or mathematically, it is a field with zero curl. This means that the electric field is a gradient of a scalar potential. For the sake of analysis, the electric field can be written as having rotational and non-rotational parts:

$$\mathbf{E} = \mathbf{E}^{(r)} - \nabla\Phi, \quad (33)$$

When the coupling between the acoustic and electromagnetic waves vanishes, the rotational part of the electric field, namely $\mathbf{E}^{(r)}$, reduces to a purely electromagnetic wave as expected. That is:

$$\nabla \cdot \epsilon^S \cdot \mathbf{E}^{(r)} = \mathbf{0}. \quad (34)$$

The use of the quasistatic assumption simplifies the piezoelectric equations, and the set of equations (27)- (30) becomes:

$$0 = \nabla \times \mathbf{H} = \frac{\partial \mathbf{D}}{\partial t} = \frac{\partial}{\partial t} (\epsilon^T \cdot \mathbf{E} + \mathbf{d} : \mathbf{T}), \quad (35)$$

$$\nabla_s \mathbf{v} = \frac{\partial \mathbf{S}}{\partial t} = \frac{\partial}{\partial t} (\mathbf{d}' \cdot \mathbf{E} + \mathbf{s}^E : \mathbf{T}), \quad (36)$$

$$\nabla \cdot \mathbf{T} = \rho \frac{\partial \mathbf{v}}{\partial t} - \mathbf{F}. \quad (37)$$

Discretization of these equations is necessary for a numerical treatment of waves propagating in piezoelectric materials. Physics-based models take on the discretization of these equations using various techniques. Chapter 3 is dedicated to the study of various models used for approximating the solutions of these equations. Phenomenological models are typically not directly concerned with the elastodynamic equations given above, and use instead other equations for wave modeling. This will be reviewed in Chapter 3.

2.8 Solutions of the Elastodynamic Equations

Here the possible solutions of the combined piezoelectric and electromagnetic differential equations are reviewed in some detail. This provides insight into the

behaviour of the elastodynamic waves in piezoelectric solids. Often, the simplest means of studying the wave propagation phenomena, is to consider plane wave solutions of the differential equations.

2.9 Christoffel's Equation and Slowness Curves

As previously mentioned, the combined piezoelectric and Maxwell's equations have in general five solutions. The acoustic wave equations have three uniform plane wave solutions for each propagation direction, and the electromagnetic wave equations have two [5]. These solutions are in general not independent but coupled through the piezoelectric constitutive equations discussed above. As such, each propagation direction can in general have up to five coupled wave equations, describing the physics of the particle perturbation.

2.10 Wave Equation in Solids

In order to find the equation of the waves travelling in a piezoelectric material, it is simpler to first eliminate either \mathbf{T} or \mathbf{v} from the acoustic field equations below:

$$\nabla \cdot \mathbf{T} = \rho \frac{\partial \mathbf{v}}{\partial t} - \mathbf{F}, \quad (38)$$

$$0 = \nabla \times \mathbf{H} = \frac{\partial \mathbf{D}}{\partial t} = \frac{\partial}{\partial t} (\epsilon^T \cdot \mathbf{E} + \mathbf{d} : \mathbf{T}), \quad (39)$$

$$\nabla_s \mathbf{v} = \mathbf{s}^E: \frac{\partial \mathbf{T}}{\partial t}. \quad (40)$$

where \mathbf{F} is the external body force (generally not present unless the body is subjected to external stresses.) But for the sake of completeness, \mathbf{F} is retained here.)

Acoustic wave equations are then derived by eliminating either \mathbf{T} , or \mathbf{v} from the acoustic field equations and constitutive relations. The preferred approach is to eliminate \mathbf{T} as it contains 6 variables, instead of \mathbf{v} which only contains three [5].

In order to do this elimination, equation (38) is first differentiated with respect to time:

$$\nabla \cdot \frac{\partial \mathbf{T}}{\partial t} = \rho \frac{\partial^2 \mathbf{v}}{\partial t^2} - \frac{\partial \mathbf{F}}{\partial t}, \quad (41)$$

and equation (40) is multiplied by the stiffness matrix:

$$\mathbf{c}: \nabla_s \mathbf{v} = \frac{\partial \mathbf{T}}{\partial t} \quad (42)$$

The equation of the acoustic wave can now be found in terms of \mathbf{v} by replacing the time derivative of \mathbf{T} in equation (39) into (41):

$$\nabla \cdot \mathbf{c}: \nabla_s \mathbf{v} = \rho \frac{\partial^2 \mathbf{v}}{\partial t^2} - \frac{\partial \mathbf{F}}{\partial t} \quad (43)$$

This equation can be written in matrix form with abbreviated subscripts as:

$$\nabla_{iK} \cdot \mathbf{c}_{KL} \nabla_{Lj} \mathbf{v}_j = \rho \frac{\partial^2 \mathbf{v}}{\partial t^2} - \frac{\partial \mathbf{F}}{\partial t} \quad (44)$$

where $i, j = x, y, z$, and $K, L=1,2,3,4,5,6$.

As the discretization problem here will not involve external forces, \mathbf{F} will be henceforth left out. The matrix differential operators ∇_{iK} , and ∇_{Lj} are

defined as:

$$\nabla_{iK} = \begin{bmatrix} \partial/\partial x & 0 & 0 & 0 & \partial/\partial z & \partial/\partial y \\ 0 & \partial/\partial y & 0 & \partial/\partial z & 0 & \partial/\partial x \\ 0 & 0 & \partial/\partial z & \partial/\partial y & \partial/\partial x & 0 \end{bmatrix}$$

$$\nabla_{Lj} = \text{transpose}(\nabla_{iK})$$

Since a uniform plane wave traveling along an arbitrary direction $\hat{\mathbf{l}} = \hat{x}l_x + \hat{y}l_y + \hat{z}l_z$ is sought here, which is of the form: $e^{i(\omega t - k \cdot \hat{\mathbf{l}})}$, resulting the simplified forms of ∇_{iK} , (and the transposed form ∇_{Lj}):

$$-ik \begin{bmatrix} l_x & 0 & 0 & 0 & l_z & l_y \\ 0 & l_y & 0 & l_z & 0 & l_x \\ 0 & 0 & l_z & l_y & l_x & 0 \end{bmatrix},$$

This will give the simplified wave equation :

$$k^2(l_{iK}c_{KL}l_{Lj})v_j = k^2\Gamma_{ij}\rho v_j = \rho\omega^2 v_i. \quad (45)$$

known as the Christoffel's equation.

For example, for an isotropic solid, Christoffel's tensor becomes:

$$[\Gamma_{ij}] = \begin{bmatrix} c_{11}l_x^2 + c_{44}(1 - l_x^2) & (c_{12} + c_{44})l_x l_y & (c_{12} + c_{44})l_x l_z \\ (c_{12} + c_{44})l_x l_y & c_{11}l_y^2 + c_{44}(1 - l_y^2) & (c_{12} + c_{44})l_y l_z \\ (c_{12} + c_{44})l_x l_z & (c_{12} + c_{44})l_y l_z & c_{11}l_z^2 + c_{44}(1 - l_z^2) \end{bmatrix}. \quad (46)$$

As it can be seen, the Christoffel tensor Γ_{ij} , is only a function of the propagation direction, and that of the propagation medium's stiffness constant c_{KL} . Equation (45) holds for all materials, whether isotropic or anisotropic [7].

In general, there can be three orthogonal polarizations for each propagation direction of a given crystal. These waves do not necessarily travel with the same phase velocity. In addition, the displacement vector can have any arbitrary angle with the propagation vector.

Analytical solutions of equation (45) are only available in special cases. That is, only when the determinant of Γ_{ij} , can be factorized into a product of polynomials in terms of velocity. This is possible when two of the three non-diagonal entries of the Christoffel

tensor become zero. In all other cases numerical solutions of the equation have to be used. Such is the case for most wave propagation problems in piezoelectric media.

To identify the solution set, the inverses of the wave velocities are plotted. Referred to as slowness surfaces, there are generally three such surfaces for the three waves previously mentioned (one called quasi-transverse and the two other are termed quasi-longitudinal). The slowness surfaces are particularly important in reflection problems at the boundaries, and they relate to Snell's law [5].

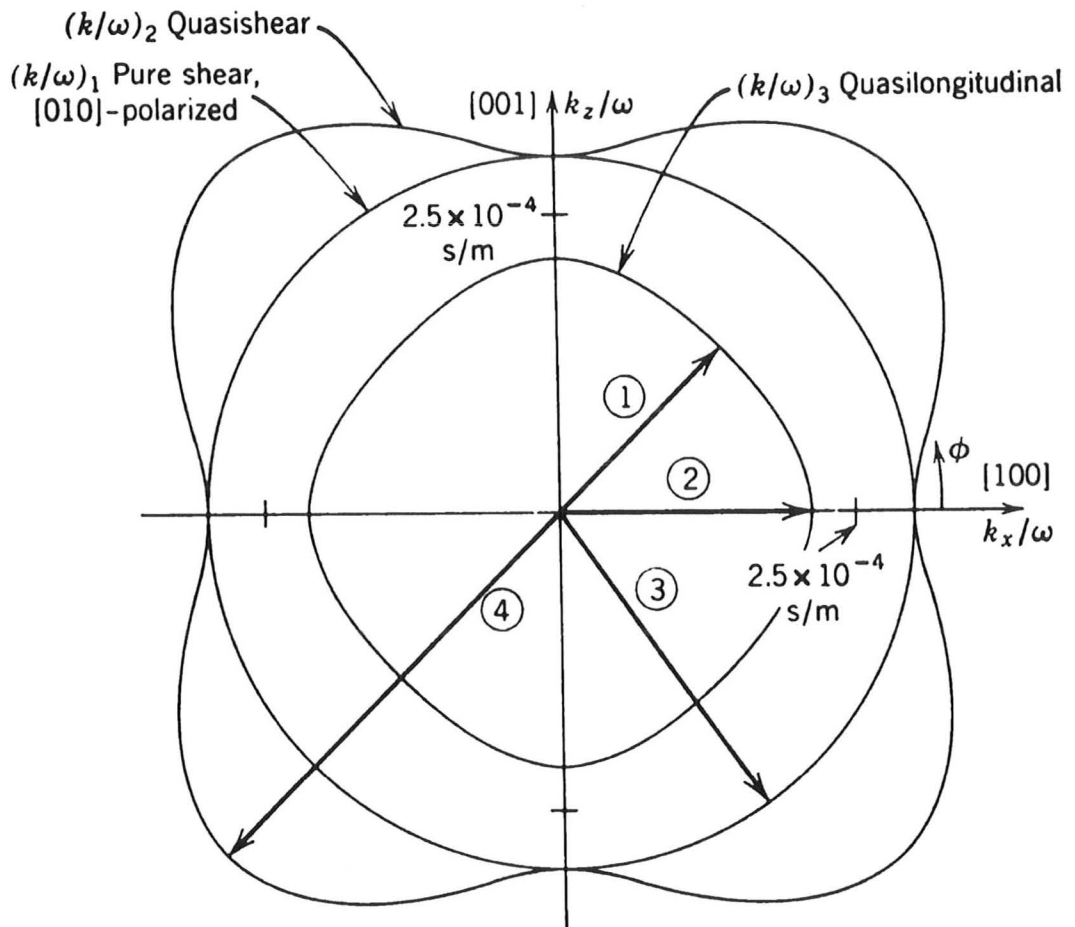


Figure 4 A Sample Slowness Curve for a Cubic Crystal (GaAs) [5]

Figure 4 shows a sample slowness curve for gallium arsenide which belongs to the cubic crystal group. For simplicity the effects of piezoelectricity (which change the curves only slightly,) have been ignored.

Chapter 3: SAW Devices and Device Modeling

3.1 Anatomy of a Typical SAW Device

SAW devices were long known before piezoelectric materials were used to generate them. The application of SAWs in electronics was initiated in 1965 by White and Voltmer at the University of California, at Berkeley [1]. This was accomplished through the invention of the interdigital transducer (IDT), which is a thin metallic structure deposited on the surface of piezoelectric materials (Figure 5). Other structures such as reflectors, and directional IDTs were later developed for interacting with, and manipulating the surface waves.

The most basic IDT is comprised of two comb-like structures inserted into one another without touching. (Figure 5). When an alternating voltage is applied to the metallic structure, the electric signal creates surface charges that are converted into mechanical stresses by the piezoelectric substrate. (In the previous chapter, the piezoelectric process governing this energy conversion was discussed.) The resulting stress causes a deformation in the solid, launching a wave on the surface of the material. If the polarity of the applied signal is periodically changed, the resulting strain also changes sign, generating a wave such a Rayleigh wave.

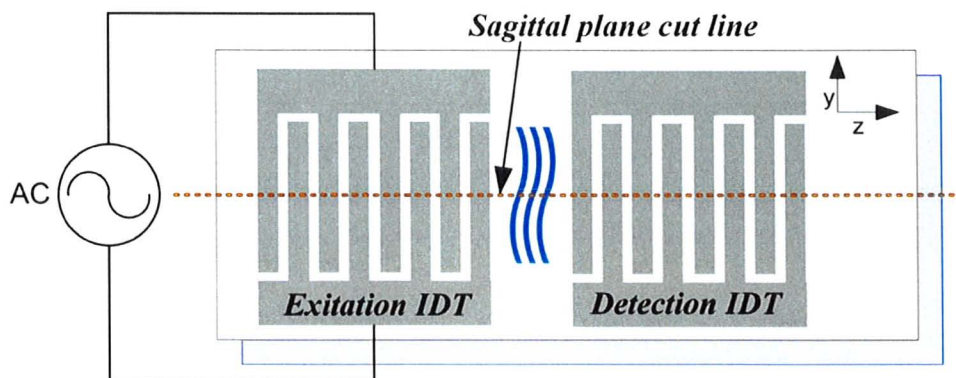


Figure 5 SAW generation and Detection using IDTs

The acoustic waves generated in the fashion explained above, undergo partial reflections at discontinuities and imperfections of the substrate. If these imperfections are not planned for, the result is a random reflection pattern, which dissipates the wave energy every which way. However, by placing reflectors on the path of the propagating wave at integer multiples of the wavelength, it is possible to cause these reflections interact constructively so that the end result of several partial reflections is a significant reflection of the original wave. As well, the energy of the wave will remain concentrated in a region close to the surface of the substrate.

3.2 Reflector-Based SAW Applications

The reflection mechanism mentioned above, allows for creation of endless configurations for different applications. Let us note that, in the presence of reflectors, the input and output IDT can be combined into one. Using this scheme a periodic signal of a

short duration is applied to the IDT, launching an acoustic wave. This wave then travels along, and upon encountering reflectors, is partially reflected back towards the IDT. When several reflectors are placed in the path of a wave, several reflections are sent back in the direction of the IDT. When a unique pattern of reflectors is created, the device can be used as an identification tag, whereby a signal detection circuit connected to the IDT can identify this pattern as a number, similar to a barcode.

A typical SAW device generally includes IDTs, reflectors and gaps. Figure 6 shows a device consisting of an IDT with reflectors on both sides.

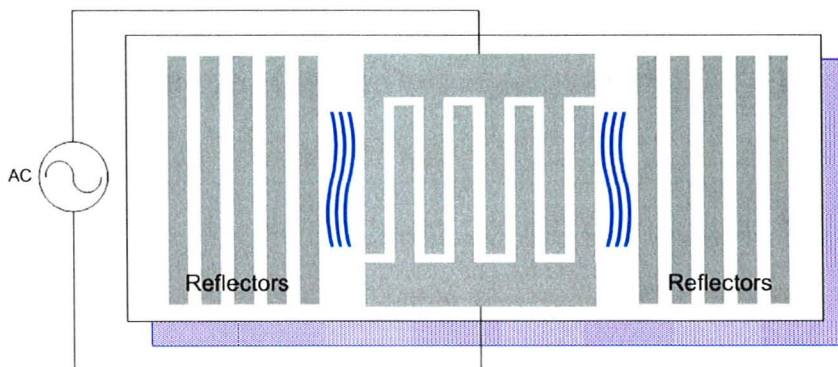


Figure 6 IDTs on a SAW Device

The IDT is separated by a gap from the reflectors, and the reflectors are typically grounded to avoid the regeneration of SAW waves.

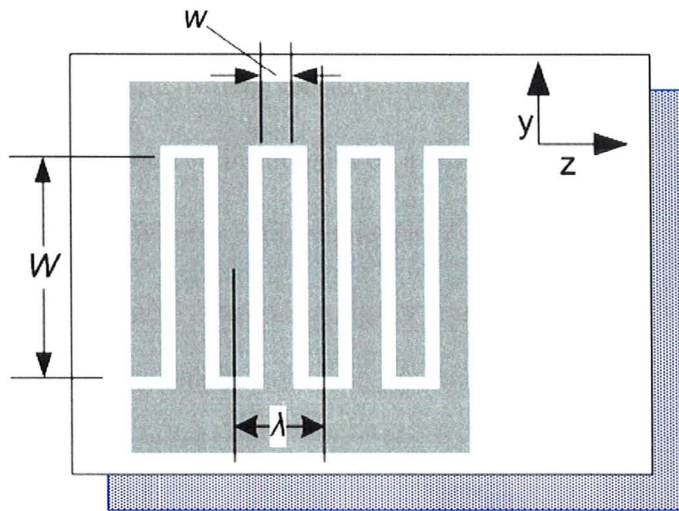


Figure 7 SAW Structure Characteristic Lengths

Figure 7. shows the characteristic lengths of an IDT. The overlap of the opposite side fingers of the IDT is the called device aperture often denoted by W , the period p_I is defined as the distance containing two metallic strips which is also equal to the wavelength λ as shown. The periodicity is defined as $p = p_I/2$. The ratio of the finger width w to p is typically referred to as the metallization ratio, denoting the thickness of the structure. The metallization ratio becomes important for thick structures, as the mass-loading effect will interfere with the vibrational patterns of the free substrate surface.

In this configuration, an alternating electric signal with a frequency f , applied to the IDT, launches an acoustic wave with a wavelength λ . Similar to the IDT structure, the reflectors can have their own period, and operate at a frequency $f_{ref} = v_{SAW}/(2 p_{ref})$, which need not be (but generally is) the same as the IDT and other SAW components. A reflector typically reflects around its own frequency f_{ref} . If an IDT is surrounded on both

sides by two reflectors, it is possible to effectively create a standing wave, and trap the acoustic energy with the frequency close to f_{ref} .

The periodicity of the grating has another energy storing effect in addition to the wave confined to the surface. The traveling surface acoustic wave is not only reflected within the surface, but it is also reflected into the bulk of the material. Most of the reflected wave into the bulk of the material interferes destructively, and has little energy loss or energy storing effect. However, around f_{ref} this interference becomes constructive and the acoustic energy is stored close to the surface. By the same token, continuity of a periodic structure is imperative for keeping the losses low and maintaining the energy-storing effect. Thus, losses are significantly reduced by replacing gaps with periodic structures of the right periodicity. [8],[9].

3.3 Frequency of Operation of SAW Devices

The speed of propagation of sound in a given medium is determined by the material. For anisotropic materials this speed is generally dependent on the direction of propagation. The relation connecting this speed with the frequency of the vibrations is:

$$\lambda = \frac{v}{f} \quad (47)$$

Where λ is the wavelength of the acoustic wave and f is the frequency of the excitation propagating in the medium. As previously mentioned, the wavelength of the SAW is defined by specifying the geometry of the IDT, and that of the reflectors.

3.4 Domain of Simulation

Figure 5 shows the symmetry of the device with respect to a line denoted as the “sagittal plane cut line.” When the device aperture W , is large enough compared to λ , the structure can be considered infinite in the y direction. This permits the reduction of the problem to two dimensions, whereby the dependence on y is removed.

The domain of study then becomes the plane whose intersection with the zy plane, is the dotted line shown in Figure 5. This plane will be referred to as the sagittal plane, and for a region containing only one IDT finger, the computational domain becomes that depicted in Figure 8.

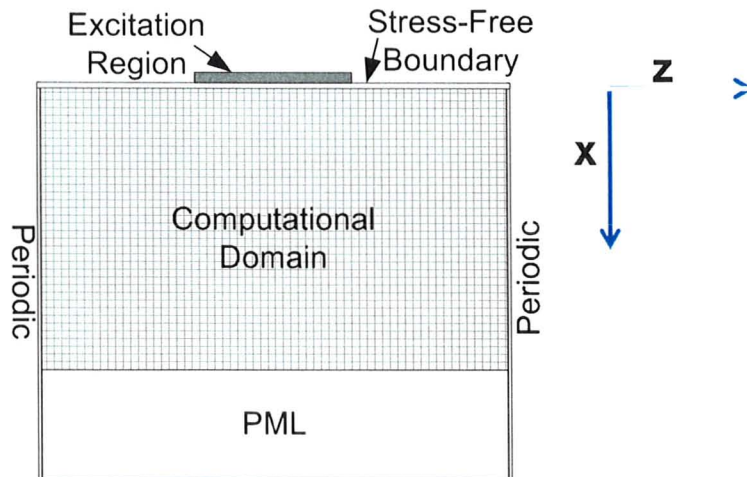


Figure 8 Domain Representing One IDT Finger on the Sagittal Plane

The periodic boundary conditions shown in Figure 8 simply mean that the domain repeats itself infinitely on the left and right. As for the rest of the boundaries noted, they will be discussed in detail below.

3.5 Review of Available Methods and Simulation Techniques

The chief objective of this research was to improve on the available techniques in implementing an efficient FDTD SAW simulator [10]. This includes the discretization of the electroacoustic equations discussed in Chapter 2, and the advanced boundary conditions required to fully describe the physical system. The latter is the topic of Chapter 4.

First a review of existing numerical techniques, currently in use for modeling SAW devices, is given.

3.5.1 Rigorous vs. Phenomenological Techniques

For the design of high performance SAW devices, accurate modeling and simulation techniques are essential. Although rigorous (or physics-based methods) provide the highest accuracy, time constraints often render such methods impractical. For this reason, several phenomenological methods have been proposed and developed. In light of the periodicity of these devices, a departure from the physics-based models becomes possible under certain conditions. Several innovative models have been designed making use of this harmonic feature. The most successful of these methods employ the concept of harmonic admittance, developed by Bløtekjær et al. and explained in [11],[12]. This method was later reformulated by Zhang et al. [13]. By employing this method, it is possible to obtain the harmonic device admittance and the dispersion relationships using only a small segment of the device.

3.5.2 Development of Approximate Field-Theoretical Formulations

In Chapter 2, the details of the governing differential equations required for the development of field-theoretical formulation were discussed. We will now turn to the discretization of these differential equations, and the various numerical techniques used for solving them.

Several approximations and appropriate boundary conditions have to be considered. First, it is noted that the acoustic wave velocities are very much slower than the speed of electromagnetic radiation. When the acoustic wave perturbation is the

dominant mode, in comparison by the electromagnetic waves, it is possible to resort to the quasistatic approximation, with little loss of accuracy.

Another appeal of the quasistatic approximation is that the inclusion of the electromagnetic waves would require timesteps so small, that the simulation would simply take too long. It must be noted that size of the timestep is also a stability requirement for the simulation. For example, in a 2D FDTD simulation, the Courant stability criterion requires [29]:

$$\Delta t \leq \frac{\Delta x}{\sqrt{2}v_{max}} \quad (48)$$

Where v_{max} is the speed of propagation of the wave in the medium. It can be seen that if the speed of light it used, the timestep becomes very small.

3.6 Boundary Condition Considerations

In modeling SAW devices, the substrate is generally considered to be semi-infinite ($z < 0$ halfspace), which, because of the low penetration depth of the waves is a satisfactory approximation. It must be noted that this is the case only when pure surface acoustic waves are launched on the surface, and there are no imperfection, discontinuities, or reflectors present. In the presence of any of these structures, there will indeed be reflections which will radiate acoustic energy into the substrate causing further reflections from the bottom of the device. These unwanted reflections will interfere with the device

response, unless an absorbing boundary condition is used to suppress them. Chapter 4, which includes the essential portion of this Masters research is dedicated to the absorbing boundary conditions in order to remove any unwanted reflections.

The deposited metallic strips on the surface are assumed to be infinitely thin as far as the charge accumulation is considered. There are also situations when the mechanical mass-loading effects due to the weight of the metallic layer have to be included.

For the sake of completeness both electrical and mechanical boundary conditions will be stated below [14]:

The mechanical boundary conditions are:

- 1- The acoustic (mechanical) displacement field is continuous across the electrode-substrate boundary,
- 2- The normal component of stress is continuous across the electrode-substrate boundary,
- 3- On the free substrate surface, the normal component of stress vanishes.

The electrical boundary conditions are:

- 1- The electric potential has no discontinuities,

- 2- Inside the metallic electrodes, the electric potential is constant,
- 3- On the free substrate the surface charge density must vanish,
- 4- The system is charge neutral.

Furthermore, we assume that there is no radiation on the surface. And that the source of excitation is always and only from the electrodes by means of an applied electric potential [14]. As well, it is assumed that there is no radiation (of the mechanical or electromagnetic nature) from inside the substrate towards the surface.

With these assumptions, the described system can be modeled. In order to extract the desired characteristic response, what remains is to solve for the fields under an excitation, and to obtain the total surface charge density over the electrode-substrate interface.

Some phenomenological techniques also use this produced harmonic (oscillating) net charge, to find the harmonic admittance.

3.7 Current State of Work on Solutions of Numerical Field Equations

There are currently several numerical methods suggested for field equations described. The most successful approaches involve one or a combination of below techniques. References containing detailed description of each approach are given for each approach:

Frequency-domain techniques:

- 1- Finite Element Method (FEM) [15],[16].
- 2- Space harmonics expansion [17].
- 3- Green's function [18][19].
- 4- Boundary element method [20]-[28]
- 5- Both FEM and space harmonics expansion [29]

Time-domain techniques:

- 6- Finite Difference Time Domain (FDTD) [30].

3.8 Finite difference method (FDTD)

FDTD has long been used for the analysis of the propagation of electromagnetic waves. Maxwell's equations are discretized in time and space, and solving this system yields the solution for the wave. Several improvements have been made over the years to enable efficient calculation of the solution. One particular advancement is attributed to Yee's algorithm which, through the use of an ingenious grid system, provides a very robust basis [31].

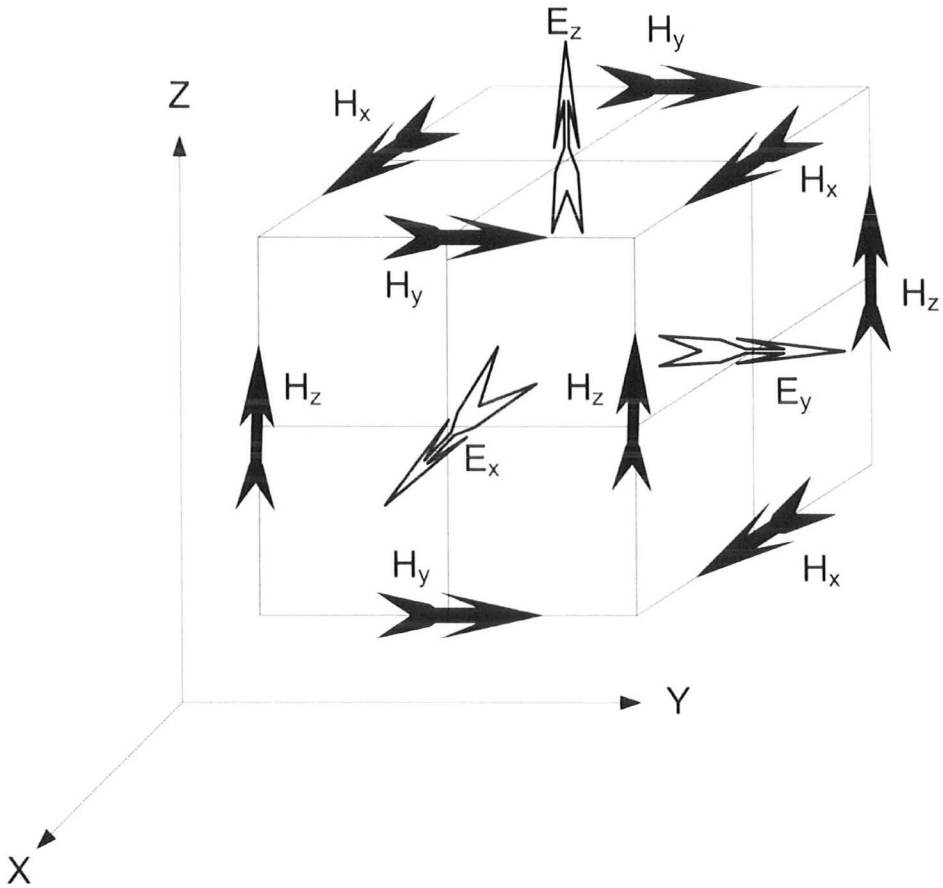


Figure 9 Yee's Leapfrog Algorithm

Figure 9 provides the essence of this method for simulating the electromagnetic waves, where \mathbf{E} and \mathbf{H} components are centered in the three dimensional space; every \mathbf{H} component is surrounded by four \mathbf{E} components, and conversely every \mathbf{E} component is surrounded by four \mathbf{H} components. The resulting FDTD expressions are second order accurate and are central-difference. The complete finite difference equations of Maxwell can be found in [32].

As far as elastodynamic equations presented in Chapter 2 are concerned, which describe the acoustic and Maxwell's equations, a parallel situation can be worked out. Using this scheme and noting that the velocity vector \mathbf{v} is the analog of \mathbf{H} , and \mathbf{T} is the analog of \mathbf{E} , a similar algorithm can be found to discretize the elastodynamic set of equations. This has been demonstrated in [10] and shown in Figure 10.

The advantages of a time-domain technique such as FDTD are manifold. It might be desired to obtain the broad-band frequency response of a SAW structure. This can be achieved using a time-domain technique, and an impulse excitation. Visual wave propagation tools can also be implemented in an FDTD simulator with relative ease. Using Yee's approach as described, efficient parallel processing techniques can be implemented into the simulator. The code implemented here which incorporates these features is visually summarized in Figure 11.

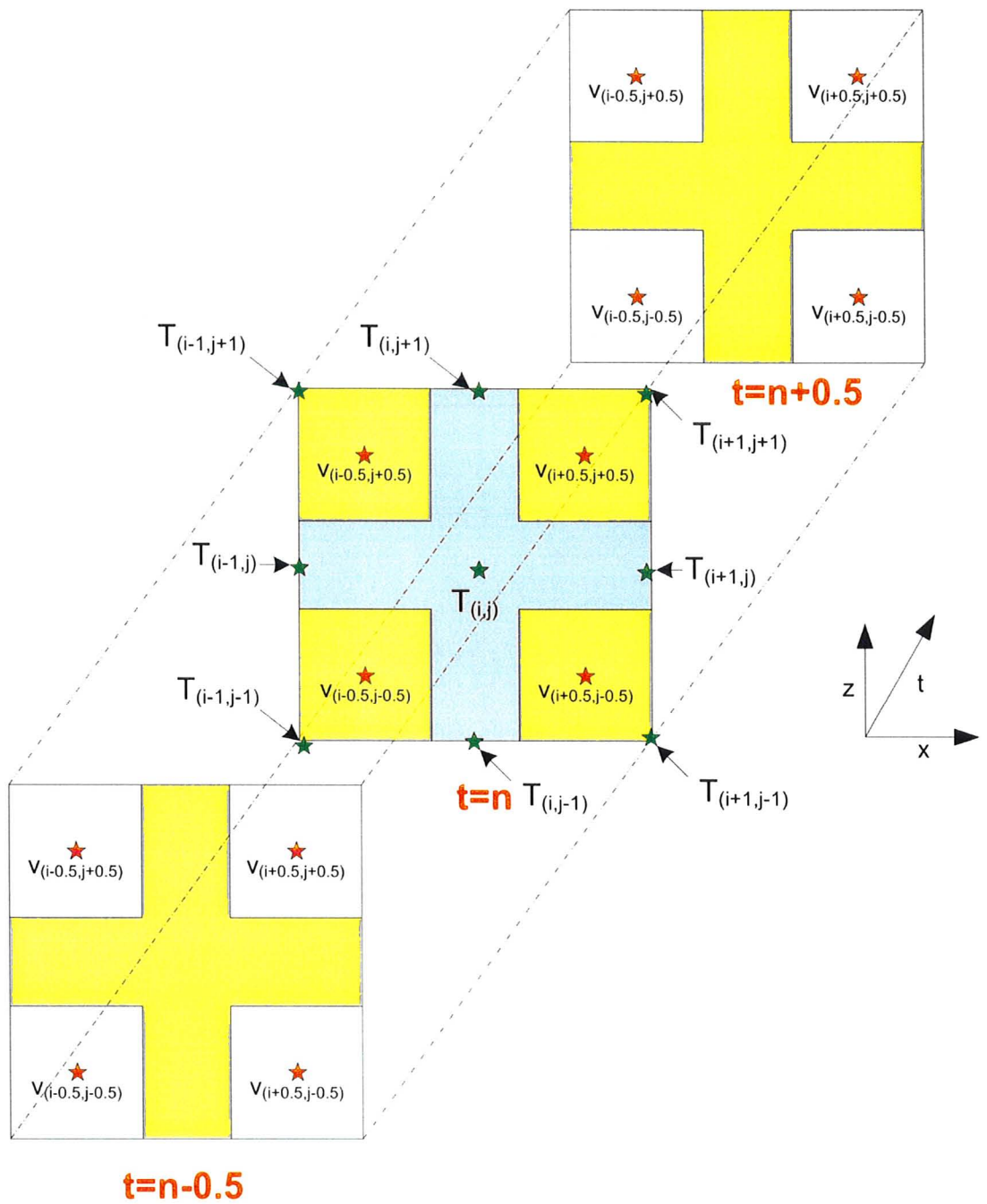
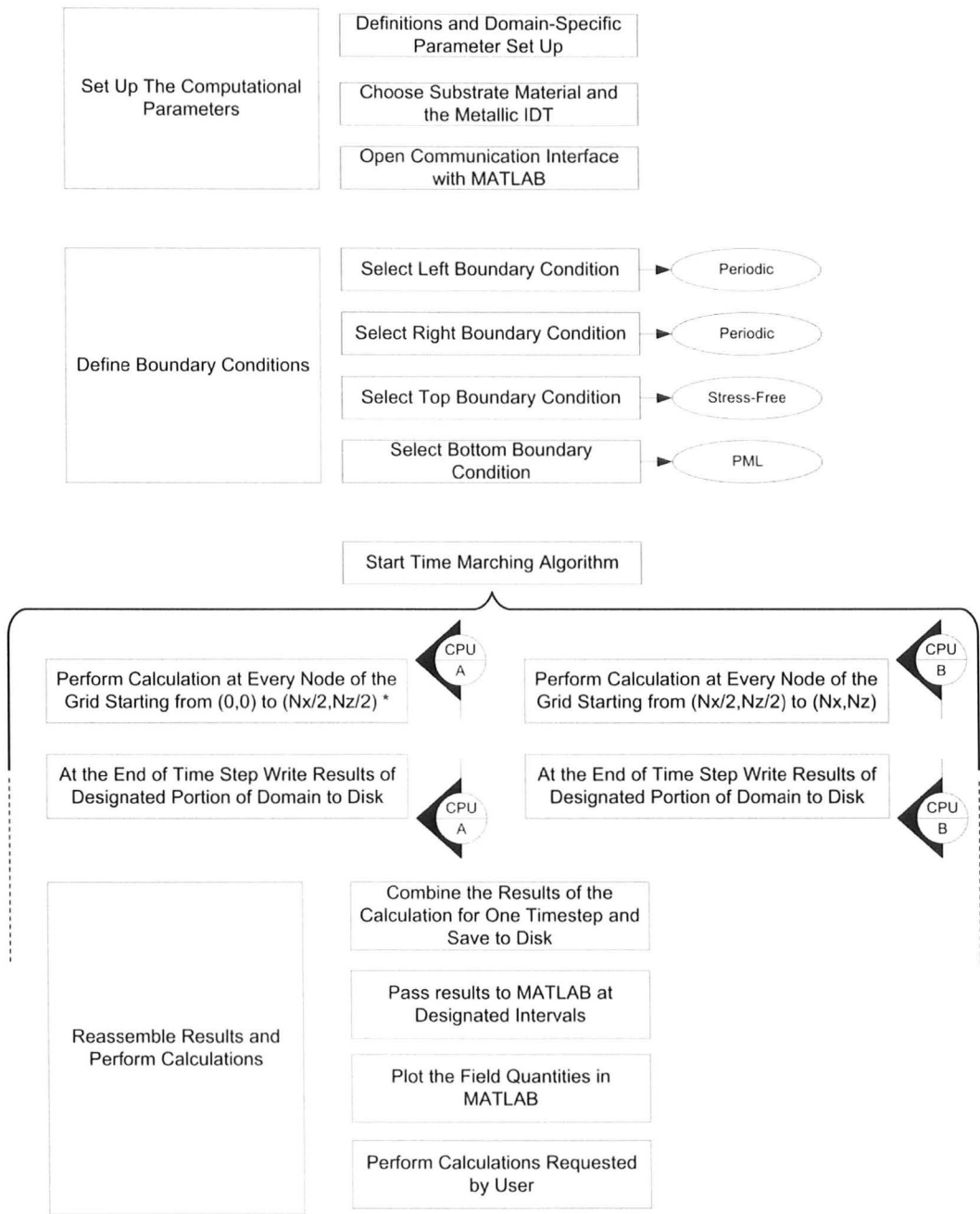


Figure 10 Staggered Stress and Velocity Field Values Based on Yee's- Approach for Simulation of Electromagnetic Waves

By assuming that the device is infinitely periodic, the computational domain can be reduced to one period of the device. Since most devices are long compared to the wavelength of the SAW and generally include tens of fingers, the preceding assumption is justified. This simplifies the computational domain by solving the equation only for one period. Although, the details of the Yee's algorithm have been spared in this analysis, it is well known that Yee's approach is particularly suitable for parallel processing. Each point on the grid can be calculated based only on, the grid values from the previous timestep. This will enable for instance, several processors to run in parallel and collate their data once at the end of a single timestep (Figure 11.) Reference [32] provides a complete description of this approach for the electromagnetic case. These considerations make FDTD, and the extension of current work a potentially powerful technique for the analysis of SAW devices.

3.9 The FDTD Simulator

The FDTD simulator used in this work is implemented in C++ with a MATLAB engine interfaced for real-time plotting of the field values. Figure 11 depicts the block diagram of the simulator program, outlining the important features discussed in the preceding and current chapters, and the treatment of boundaries using the perfectly matched layer discussed in the next chapter.



* N_x, N_z are the number of points used for spatial discretization in the x and z direction

Figure 11 Block-Diagram of the Implemented SAW FDTD Simulator in C++

The absorbing boundary conditions, in particular the perfectly matched layer for the elastodynamic problem will be discussed next.

Chapter 4: Absorbing Boundary Conditions

4.1 Review of the Existing Boundary Conditions for Acoustic Waves

Several absorbing boundary conditions (ABCs) have been introduced for acoustic waves, with progressive improvements. Most of these ABCs were originally developed for electromagnetic wave propagation, and the majority were developed in the frequency-domain. In Chapter 3, the strengths of time-domain methods were highlighted. The main focus of this work will be on the time-domain ABC boundary conditions.

In his 1994 paper, Bérenger described a new boundary called the perfectly matched layer (PML) for electromagnetic waves, which offered significant improvements over previous ABCs [33].

As previously stated, frequency domain modeling methods have enjoyed a more developed set of domain termination techniques, including ABCs and the PML.

In a pioneering work in 1996, Chew and Liu developed a PML for elastodynamics [34]. In 2006, Chagla and Smith introduced a PML for piezoelectric materials by splitting the velocity components into normal and tangential subcomponents. The resulting absorbing boundary condition showed instabilities for some crystal classes [10].

Here, we apply the PML to anisotropic materials, which include all piezoelectric crystals, and show numerical measures of the PML for SAWs. It is further shown that the instabilities are removed by introducing a matching condition.

4.2 Review of the Absorbing Boundary Conditions for Electromagnetic Waves

The ABC equations for the electromagnetic waves are:

$$\epsilon_0 \frac{\partial \mathbf{E}}{\partial t} + \sigma \mathbf{E} = \nabla \times \mathbf{H} \quad (49)$$

$$\mu_0 \frac{\partial \mathbf{H}}{\partial t} + \sigma^* \mathbf{H} = -\nabla \times \mathbf{E} \quad (50)$$

where σ is the conductivity and σ^* is a non-physical quantity introduced to symmetrise the absorption of the magnetic field with that of the electric field [36]. ϵ_0 , and μ_0 are the permittivity and permeability of the free space, respectively.

The matching condition in Bérenger's derivation is defined as [36]:

$$\frac{\sigma}{\epsilon_0} = \frac{\sigma^*}{\mu_0} \quad (51)$$

Equation (51) states that the ratios of loss-coefficients are the same as the ratios of the corresponding field coefficients. This relation, also referred to as the impedance matching equation, ensures that the impedance of the wave travelling inside the domain, matches

that of the lossy ABC medium defined by equation (49) and equation (50). The result is a reflectionless propagation of a normally incident plane wave as it passes through the interface. This works well at normal incidences but the reflection becomes large at grazing angles.

Bérenger addressed this problem, by splitting the field quantities into normal and tangential components and modifying equation (49) and equation (50) for a TE mode electromagnetic wave, (where the \mathbf{E} field is in the xy plane, and the \mathbf{H} field is parallel to the z direction.) The reflection coefficient with $n = 1$ for vacuum, matched to this newly defined lossy medium is given by:

$$r = \left(\frac{1 - \cos\theta}{1 + \cos\theta} \right)^n \quad (52)$$

This reflection coefficient is zero for both normal and grazing incidence.

A fictitious medium is subsequently defined by: [36]

$$\epsilon_0 \frac{\partial E_x}{\partial t} = \frac{\partial(H_{zx} + H_{zy})}{\partial y} \quad (53)$$

$$\epsilon_0 \frac{\partial E_y}{\partial t} + \sigma E_y = \frac{\partial(H_{zx} + H_{zy})}{\partial x} \quad (54)$$

$$\mu_0 \frac{\partial H_{zx}}{\partial t} + \sigma^* H_{zx} = - \frac{\partial E_y}{\partial x}$$

$$\mu_0 \frac{\partial H_{zy}}{\partial t} = \frac{\partial E_x}{\partial y} \quad (55)$$

The subcomponents of the \mathbf{H} field in the z direction are denoted as H_{zx} and H_{zy} . This is a generalization of the physical electromagnetic equations as a linear combination of the normal and tangential components. By defining the \mathbf{H} field in this manner, it is possible to absorb the normal component of the wave, whilst the tangential component freely propagates without loss in the medium. Reference [36] provides a detailed derivation of the PML for electromagnetic waves.

4.3 PML for Elastodynamic Waves

Before presenting the derivation of the PML for elastodynamic waves in anisotropic solids, the scattering problem concerning boundary conditions for such waves is reviewed.

4.3.1 A Review of Elastodynamic Wave Scattering from Boundaries

As previously stated, the combined piezoelectric and Maxwell's equations have in general five wave solutions. (The acoustic wave equations have three uniform plane wave solutions for each propagation direction, and the electromagnetic equations have two.) These solutions are in general not independent but coupled through the piezoelectric constitutive equations. In total therefore, each propagation direction has five coupled equations.

In scattering problems involving these waves, there can be up to five reflected and five transmitted waves for an arbitrary type of incident wave (Figure 12) [1].

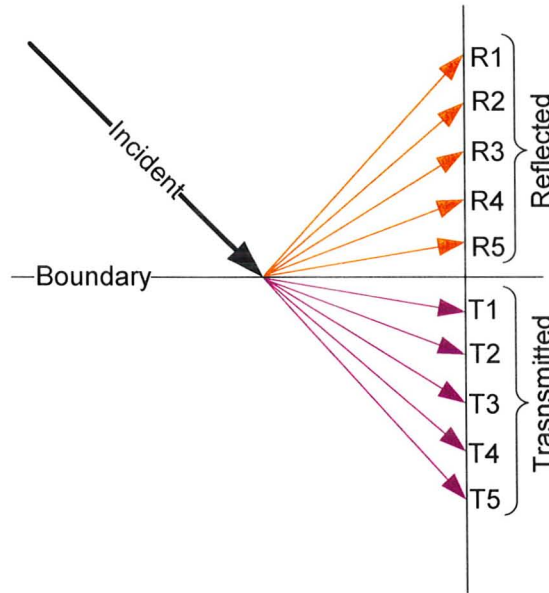


Figure 12 Boundary Scattering of Coupled Elastodynamic Waves

In equation form, the general boundary-matching results in ten component-form equations: five reflected (of the types mentioned above) and five transmitted of each kind [7].

$$\mathbf{v} = \mathbf{v}'$$

$$\mathbf{T} \cdot \hat{\mathbf{n}} = \mathbf{T}' \cdot \hat{\mathbf{n}}$$

(56)

$$\hat{\mathbf{n}} \times \mathbf{E} = \hat{\mathbf{n}} \times \mathbf{E}'$$

$$\hat{\mathbf{n}} \times \mathbf{H} = \hat{\mathbf{n}} \times \mathbf{H}'$$

where $\hat{\mathbf{n}}$ is the unit vector normal to the boundary of the two media, and the primed quantities represent the values in the medium which lie on the other side of the boundary. (i.e. transmitted wave quantities.)

The behaviour of these waves in a piezoelectric material, is determined by the type of crystal (symmetry group), the direction of propagation with respect to the crystal axes, and the crystal cut axis, which defines the plane of propagation. Propagation of the waves on specific directions—usually intentionally chosen planes of symmetry, can cause decoupling of these waves resulting in pure acoustic (or pure electromagnetic waves) in that direction. For example, on a *y*-cut lithium niobate crystal with the *z*-axis as the direction of propagation, one of the acoustic waves decouples from piezoelectricity and propagates as a purely acoustical wave. When this happens, the piezoelectric property of the crystal becomes irrelevant for the propagation of that particular mode, and the crystal simply acts as an elastic medium for the acoustic wave, as though, it were a non-piezoelectric material. The only relevance of piezoelectricity in this case, is when the wave is generated or upon its detection. The wave is usually generated, as explained in

chapter 2, by applying an electric signal to a thin metallic interdigital transducer (IDT) on the surface of the substrate.

For a decoupled acoustic wave, once the wave is launched, it travels without regard to piezoelectricity. Upon detection, the inverse of generation takes place, where the mechanical wave is converted to an electric impulse at the output IDT. In short, for pure acoustic waves, the relevance of piezoelectricity is only in the IDT regions and not in between [3].

Decoupling from piezoelectricity creates a special case of waves as mentioned; in general however, there are three acoustic waves per each direction of propagation [5]. These acoustic waves have different propagation velocities at any given direction, and they are identified, by their velocities v_1 , v_2 , and v_3 plotted as a function of propagation direction.

The slowest wave is termed (quasi-) longitudinal and the other two are called (quasi-) transverse. It is more useful as stated in Chapter 2, to represent these surfaces using the inverses of velocity values, called slowness surfaces. Such plots are very useful in studying reflection and transmission phenomena according to Snell's law, and also for determining the state of each wave at a given direction (i.e. whether the wave is evanescent or not). A line drawn from the origin denoting the direction of propagation will intersect with the three slowness curves providing the velocities of each type of wave in that direction [7].

Slowness curves are most important in choosing the ideal crystal cut angle for a given problem. This allows for example, to choose a direction in which one of the three waves is highly sensitive to piezoelectricity, while the other two are not. The excitation in that direction of the piezoelectric crystal then, yields pure waves of that mode, with minimal arousal of other types by choosing different crystal cut axes.

4.4 Derivation of the Elastodynamic PML Based on Bérenger's Approach

Here, the PML for the elastodynamic wave propagation on piezoelectric solids is derived in exact parallelism with Bérenger's formulation of the PML for electromagnetic waves [32].

The equations describing the propagation of elastodynamic waves in piezoelectric crystals are [7]:

$$\nabla_s \mathbf{v} = \mathbf{s}^E : \frac{\partial \mathbf{T}}{\partial t}, \quad (57)$$

$$\rho \frac{\partial \mathbf{v}}{\partial t} = \nabla \cdot \mathbf{T} \quad (58)$$

And

$$\mathbf{s}^E = (\mathbf{c}^E)^{-1} = \mathbf{s}^E - \mathbf{d}'(\boldsymbol{\epsilon}^T)^{-1}\mathbf{d}, \quad (59)$$

\mathbf{d} is the piezoelectric strain coefficient matrix,

\mathbf{T} is the stress vector,

\mathbf{v} is the particle velocity vector,

\mathbf{S} is the stain vector,

\mathbf{d}' is transpose of \mathbf{d} ,

\mathbf{s}^E is the 6×6 compliance coefficient matrix measures under constant electric field,

ρ is the material density,

$$(\nabla_s)' = \begin{bmatrix} \partial/\partial x & 0 & 0 & 0 & \partial/\partial z & \partial/\partial y \\ 0 & \partial/\partial y & 0 & \partial/\partial z & 0 & \partial/\partial x \\ 0 & 0 & \partial/\partial z & \partial/\partial y & \partial/\partial x & 0 \end{bmatrix}.$$

Equation (59) is called the stiffening equation to include the effects of piezoelectricity at zero displacement [7]. In component-form, the first line of equation (57), for a trigonal 3m symmetry class (to which lithium niobate (LiNbO_3) belongs,) is:

$$s_{11} \frac{\partial T_{1x}}{\partial t} + s_{12} \frac{\partial T_{2x}}{\partial t} + s_{13} \frac{\partial T_{3x}}{\partial t} + s_{14} \frac{\partial T_{4x}}{\partial t} = \frac{\partial v_1}{\partial x} \quad (60)$$

The PML is defined by introducing losses for the component field variables in equation (60). The loss terms are introduced in accordance with the existing terms in the equation, i.e.:

$$\begin{aligned}
s_{11} \frac{\partial T_{1x}}{\partial t} + s_{12} \frac{\partial T_{2x}}{\partial t} + s_{13} \frac{\partial T_{3x}}{\partial t} + s_{14} \frac{\partial T_{4x}}{\partial t} + \Psi_{T_1} T_1 + \Psi_{T_2} T_2 \\
+ \Psi_{T_3} T_3 + \Psi_{T_4} T_4 = \frac{\partial v_1}{\partial x}
\end{aligned} \tag{61}$$

where Ψ_{T_i} denote the loss terms for the corresponding stress field components.

The form of the stiffness matrix determines which components of the stress field are related through equation (60). Accordingly, the number of terms in this equation depends on the choice of substrate material. Similar to electromagnetics, equation (60) is used to develop a Bérenger-like boundary condition.

Equation (61) is likewise split into the normal and tangential subcomponents in the xz plane, (i.e. no y -dependence.) In analogy to equation (53) and (54) we have:

$$s_{11} \frac{\partial T_{1x}}{\partial t} + s_{12} \frac{\partial T_{2x}}{\partial t} + s_{13} \frac{\partial T_{3x}}{\partial t} + s_{14} \frac{\partial T_{4x}}{\partial t} + \tag{62}$$

$$\Psi_{T_1} T_{1x} + \Psi_{T_2} T_{2x} + \Psi_{T_3} T_{3x} + \Psi_{T_4} T_{4x} = \frac{\partial(v_{1x} + v_{1z})}{\partial x},$$

$$s_{11} \frac{\partial T_{1z}}{\partial t} + s_{12} \frac{\partial T_{2z}}{\partial t} + s_{13} \frac{\partial T_{3z}}{\partial t} + s_{14} \frac{\partial T_{4z}}{\partial t} = 0. \tag{63}$$

A similar hypothetical construct is required for attenuating the stress field components, together with the velocity components, while also satisfying the matching condition.

Bérenger's approach is taken here to define a matching condition based on equation (57) and equation (58), by first introducing the loss-terms explained above, to give the complete PML equations:

$$\hat{\mathbf{s}}^E \frac{\partial \mathbf{T}_x}{\partial t} + \boldsymbol{\Psi}_T \mathbf{T}_x = \nabla_{sx} \mathbf{v}, \quad (64)$$

$$\hat{\mathbf{s}}^E \frac{\partial \mathbf{T}_z}{\partial t} = \nabla_{sz} \mathbf{v}, \quad (65)$$

$$\rho \frac{\partial \mathbf{v}_x}{\partial t} + \psi_v \mathbf{v}_x = \nabla_x \mathbf{T} [\mathbf{10}], \quad (66)$$

$$\rho \frac{\partial \mathbf{v}_z}{\partial t} = \nabla_z \mathbf{T} [\mathbf{10}]. \quad (67)$$

where $\boldsymbol{\Psi}_T$ is a 6×6 non-physical loss tensor containing the stress loss-coefficients shown in equation (61) and ψ_v is a non-physical scalar denoting the velocity loss-coefficient. ∇_{sx} is the same as ∇_s except that it only contains the spatial derivatives with respect to x .

Noting that some coefficients are now tensor quantities and that $(\hat{\mathbf{s}}^E)^{-1} = \hat{\mathbf{c}}^E$, we define the acoustic matching condition as [35]:

$$\boldsymbol{\Psi}_T = \frac{\psi_v}{\rho} \hat{\mathbf{s}}^E \quad (68)$$

This relation states that the ratios between the stress and velocity loss-coefficients are the same as the ratios of the field variable coefficients. Similar to the electromagnetic case, the matching condition ensures that the loss-coefficients always maintain the same ratio, even as they progressively increase through the PML. The matrix multiplication which is new in this equation, ensures the term-wise satisfaction of the matching condition, for all components of the stress field.

4.5. Applying the Matching Condition to Derive the PML Time Update Equations

The derivation of the PML for the velocity field is less burdensome, as the loss coefficient in equation (66) are scalars. This has been previously reported as: [10]

$$\mathbf{v}_x^{n+\frac{1}{2}} = \left(\frac{2 - \Delta t \Psi_{v,i}}{2 + \Delta t \Psi_{v,i}} \right) \mathbf{v}_x^{n-\frac{1}{2}} + \frac{\mathbf{1}}{\rho} \left(\frac{\Delta t}{2 + \Delta t \Psi_{v,i}} \right) \nabla_x \mathbf{T} \quad (69)$$

However, both field variables \mathbf{v} and \mathbf{T} , have to be attenuated in accordance with a matching condition that ensures that there are no reflections from the boundary.

In order to carry this out in component form, we will work with the first row of equation (64), noting that the same analysis applies to the remaining five:

$$\begin{aligned}
 s_{11} \frac{\partial}{\partial t} T_{1x} + s_{12} \frac{\partial}{\partial t} T_{2x} + c_{13} \frac{\partial}{\partial t} T_{3x} + c_{14} \frac{\partial}{\partial t} T_{4x} + \Psi_{T1} T_{1x} \\
 + \Psi_{T2} T_{2x} + \Psi_{T3} T_{3x} + \Psi_{T4} T_{4x} = \frac{\partial(v_{1x} + v_{1z})}{\partial x}
 \end{aligned} \tag{70}$$

And the first row of the lossless equation (65) can be written as:

$$T_{1z}|_{i,j}^{n+1/2} = T_{1z}|_{i,j}^{n-1/2} - \Delta t \left(-c_{13} \frac{\partial v_3}{\partial z} \right). \tag{71}$$

Using a central difference scheme to find the time derivative, and applying the time-averaging, for unknown quantities at time n we get:

$$\begin{aligned}
 & s_{11} \left(\frac{T_{1x}|_{i,j}^{n+\frac{1}{2}} - T_{1x}|_{i,j}^{n-\frac{1}{2}}}{\Delta t} \right) + s_{12} \left(\frac{T_{2x}|_{i,j}^{n+\frac{1}{2}} - T_{2x}|_{i,j}^{n-\frac{1}{2}}}{\Delta t} \right) \\
 & + s_{13} \left(\frac{T_{3x}|_{i,j}^{n+\frac{1}{2}} - T_{3x}|_{i,j}^{n-\frac{1}{2}}}{\Delta t} \right) \\
 & + s_{14} \left(\frac{T_{4x}|_{i,j}^{n+\frac{1}{2}} - T_{4x}|_{i,j}^{n-\frac{1}{2}}}{\Delta t} \right) \\
 & + \psi_{T1} \left(\frac{T_{1x}|_{i,j}^{n+\frac{1}{2}} - T_{1x}|_{i,j}^{n-\frac{1}{2}}}{2} \right) \\
 & + \psi_{T2} \left(\frac{T_{2x}|_{i,j}^{n+\frac{1}{2}} - T_{2x}|_{i,j}^{n-\frac{1}{2}}}{2} \right) \\
 & + \psi_{T3} \left(\frac{T_{3x}|_{i,j}^{n+\frac{1}{2}} - T_{3x}|_{i,j}^{n-\frac{1}{2}}}{2} \right) \\
 & + \psi_{T4} \left(\frac{T_{4x}|_{i,j}^{n+\frac{1}{2}} - T_{4x}|_{i,j}^{n-\frac{1}{2}}}{2} \right) = \frac{\partial(v_{1x} + v_{1z})}{\partial x}
 \end{aligned} \tag{72}$$

Grouping the terms at time $n + \frac{1}{2}$ yields the time update equation:

$$\begin{aligned}
 & (2s_{11} + \Delta t \Psi_{T1}) T_{1x} |_{i,j}^{n+\frac{1}{2}} + (2s_{12} + \Delta t \Psi_{T2}) T_{2x} |_{i,j}^{n+\frac{1}{2}} \\
 & \quad + (2s_{13} + \Delta t \Psi_{T3}) T_{3x} |_{i,j}^{n+\frac{1}{2}} \\
 & \quad + (2s_{14} + \Delta t \Psi_{T4}) T_{4x} |_{i,j}^{n+\frac{1}{2}} \\
 & = (2s_{11} - \Delta t \Psi_{T1}) T_{1x} |_{i,j}^{n-\frac{1}{2}} \\
 & \quad + (2s_{12} - \Delta t \Psi_{T2}) T_{2x} |_{i,j}^{n-\frac{1}{2}} \\
 & \quad + (2s_{13} - \Delta t \Psi_{T3}) T_{3x} |_{i,j}^{n-\frac{1}{2}} \\
 & \quad + (2s_{14} - \Delta t \Psi_{T4}) T_{4x} |_{i,j}^{n-\frac{1}{2}} + 2\Delta t \frac{\partial(v_{1x} + v_{1z})}{\partial x}
 \end{aligned} \tag{73}$$

As stated above, the procedure applied to the rest of the five equations is the same, and the result can be cast into the more concise matrix form:

$$(2\hat{\mathbf{S}}^E + \Delta t \Psi_T) T |_{i,j}^{n+\frac{1}{2}} = (2\hat{\mathbf{S}}^E - \Delta t \Psi_T) T |_{i,j}^{n-\frac{1}{2}} + 2\Delta t \nabla_x \mathbf{v}. \tag{74}$$

Without loss of generality, the attenuation matrix Ψ_T is defined to contain all the corresponding loss-terms, allowing for a concise representation of the component form equations.

Making use of the matching condition defined in equation (68) to sub in for Ψ_T , results in:

$$\left(2\hat{\mathbf{S}}^E + \Delta t \frac{\Psi_v}{\rho} \hat{\mathbf{S}}^E\right) \mathbf{T}_x^{n+\frac{1}{2}} = \left(2\hat{\mathbf{S}}^E - \Delta t \frac{\Psi_v}{\rho} \hat{\mathbf{S}}^E\right) \mathbf{T}_x^{n-\frac{1}{2}} + 2\Delta t \nabla_x \mathbf{v}. \quad (75)$$

By multiplying from left by $\hat{\mathbf{c}}^E$, the time update equation within the PML becomes:

$$\mathbf{T}_x^{n+\frac{1}{2}} = \frac{\xi_v}{\xi_v^*} \mathbf{T}_x^{n-\frac{1}{2}} + \frac{1}{\xi_v^*} \hat{\mathbf{c}}^E \nabla_x \mathbf{v}. \quad (76)$$

where $\xi_v = \left(2 - \Delta t \frac{\Psi_v}{\rho}\right)$ and $\xi_v^* = \left(2 + \Delta t \frac{\Psi_v}{\rho}\right)$.

By making use of the derived matching condition given by equation (68), the quantities ξ_v and ξ_v^* become scalars, thus eliminating the need for matrix inversion. This significantly relaxes the computational burden for calculating the field values inside the PML, turning matrix algebra into simple scalar manipulation.

The end of the PML boundary is terminated with a perfect reflector. This ensures that any reflections from the terminal layer of the PML undergo a secondary attenuation upon return. This completes the PML equation for the stress field.

The matching condition is in essence a constraint, which connects the loss-coefficients of the stress and velocity fields. That is, setting Ψ_v is sufficient for defining both equation (69) and equation (76). Note that these two equations define one layer of the PML. An arbitrary number of layers can be specified, and generally the more layers the PML has, the better it is in suppressing reflections.

From one layer to the next, starting at the medium-PML interface, the loss-coefficients are gradually increased according to a profile function. At the starting layer, this loss-profile Ψ_v is small; however, it is ramped up at every layer, terminating at a final value $\Psi_{v,0}$ at the end of the PML. Generally, either a polynomial or an exponential loss profile is employed to define the sequence of Ψ_v values, as is done in electromagnetics. Here, a polynomial loss profile defined in [36] is used:

$$\Psi_{v,i} = \Psi_{v,0} \left(\frac{i - x_{PML}}{\delta} \right)^m, \quad (77)$$

where x_{PML} is the position of the onset of the PML, i is the position of each PML, δ is the thickness of the PML, $\Psi_{v,0}$ is the loss-coefficient at the terminal layer of the PML, and m is the order of the polynomial used. $\Psi_{v,0}$ is either chosen heuristically, or using an empirical formula similar to the electromagnetic PML explained in [36].

4.6 Simulation Results of the Implemented PML

4.6.1. Domain Definition and Simulation Parameters

The computational domain shown in Figure 8 is used for the discretization of the sagittal plane. The domain is terminated on the left and right sides by periodic boundaries, that model an infinite interdigital transducer (IDT). This is the case for example in a SAW resonator, where the excitation travels symmetrically in both directions.

The domain is one IDT period of the sagittal plane, with the assumption that the IDT is infinitely long compared to the wavelength of the SAW. This reduces the problem to a two dimensional analysis on the sagittal plane.

A spatial resolution of 33.57×10^{-5} m, and a temporal timestep of 0.318 ns were used on a 91×91 cell grid.

The PML was tested for sinusoidal, Gaussian, and impulse excitations. The reflection for the a sinusoidal excitation from a PML with 15 layers, placed 8 spatial steps from the PML, was less than 10^{-6} after 6000 timesteps or 19 μ s.

The implemented PML is used for the bottom of the domain. This allows any unwanted parasitic waves to be removed from the computational domain, as though the computational domain were a semi-infinite plane. Any other boundary conditions will result in spurious reflections from the bottom that will show up in the detection IDT of the device as computational noise.

The top boundary condition is stress-free, implying that all components of the stress normal to the boundary (i.e. T_1, T_5, T_6) are set to zero [30]. Therefore at the stress-free boundary, the only non-zero components of the stress are the transverse ones.

A periodic excitation with the frequency of 1GHz with a Gaussian envelope is applied to the middle of the free surface. This excitation is applied to the T_3 component of the wave which is a compressional stress component in the z-direction.

4.6.2. Results

The implemented PML was tested using Gaussian, impulse and sinusoidal excitations. As well, a host of various materials, both isotropic (i.e. non-piezoelectric media,) and piezoelectric substrates were tested. Several substrate rotations specifying the crystal cut axis and the direction of propagation were tested. The PML was stable under all these conditions, and no instabilities were seen for the classes of materials previously reported [10].

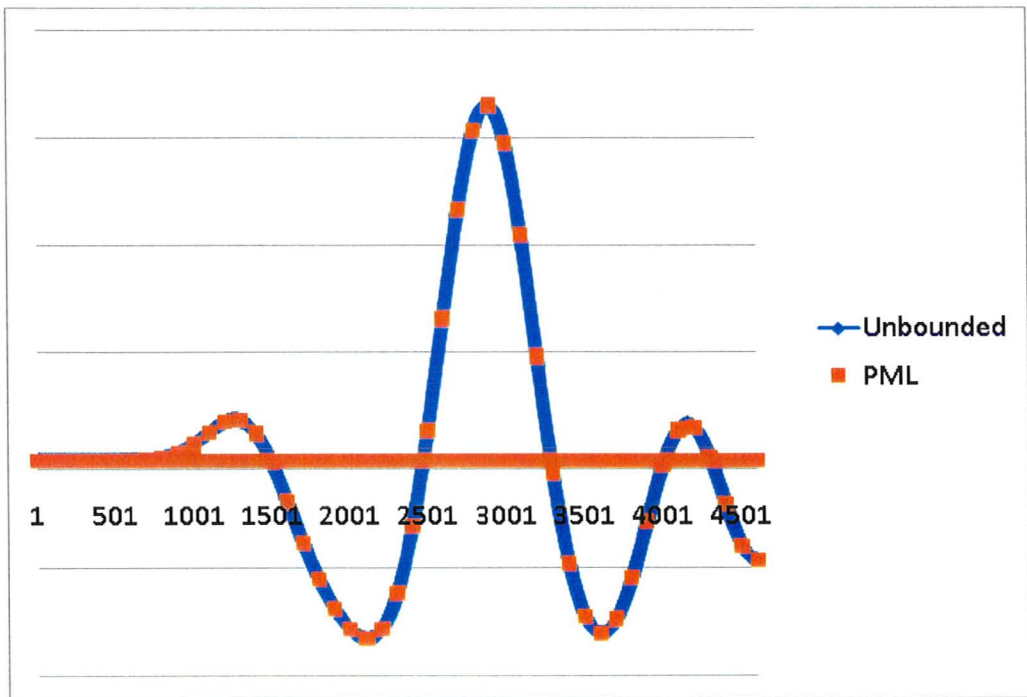


Figure 13 Comparison of the Normalized T_{xx} Field Component for an Unbounded Medium and the PML

Figure 13 shows the plot of the T_{xx} component of the field in an unbounded region, with the results of the PML superimposed on it, comparing the effectiveness of the PML in modeling an unbounded region. The difference is less than 10^{-6} % between the unbounded case and the domain terminated with the PML.

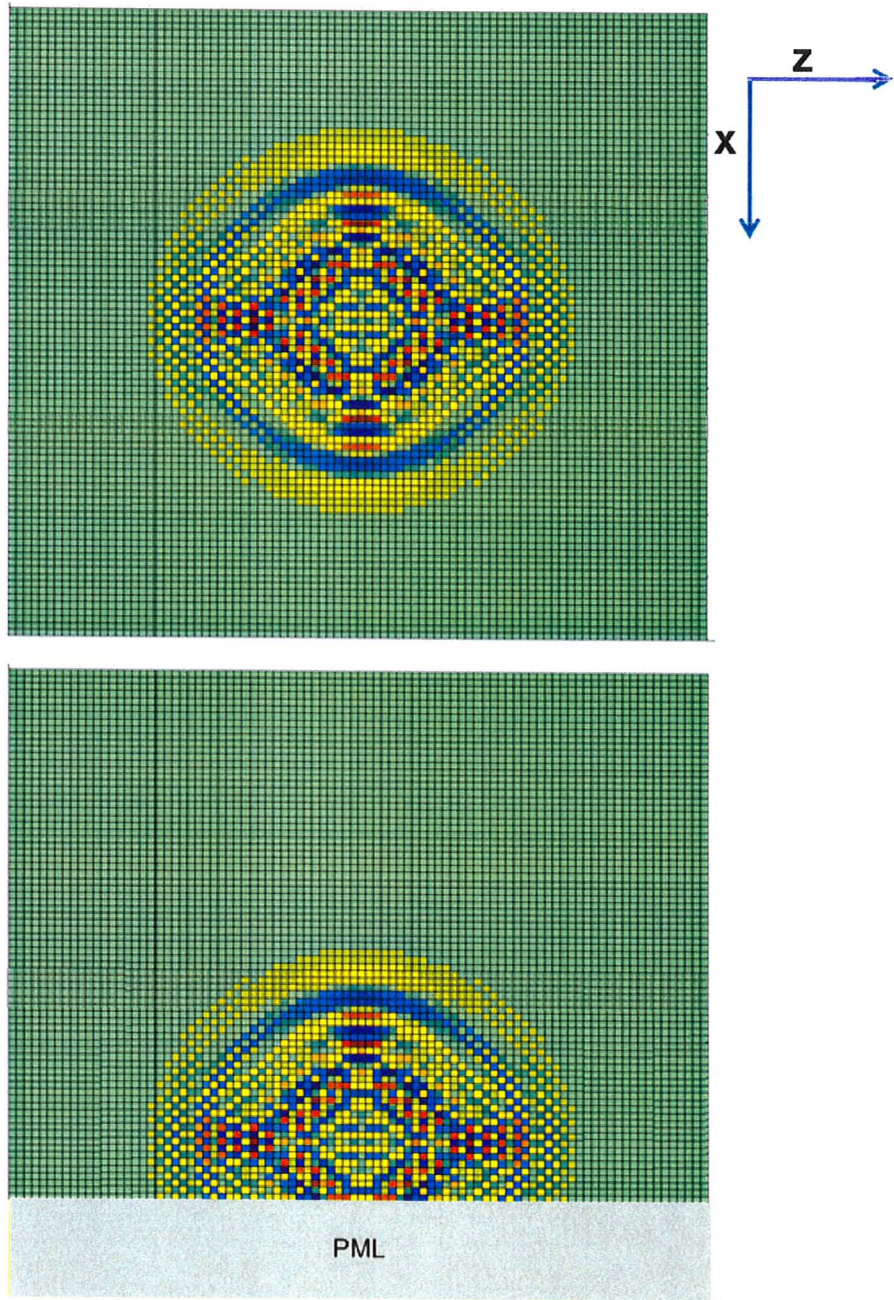


Figure 14 Excitation Near the PML. Top: A Gaussian Excitation in an Unbounded Region. Bottom: Symmetric Spread of the Same Excitation Near the PML after 15.9 μ s or 5000 Timeteps.

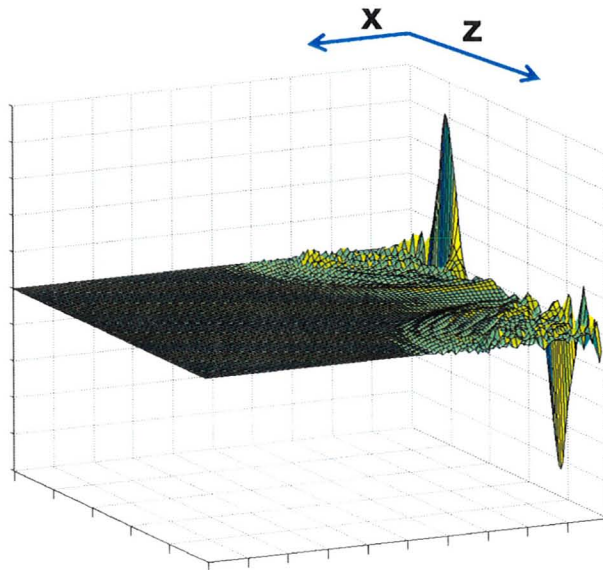


Figure 15 SAW Excitation under Metallic IDT

Figure 14 bottom, shows the excitation near the boundary after $15.9 \mu\text{s}$. The symmetric shape of the excitation is preserved even after a prolonged interaction with the PML.

Figure 15 shows the SAW launched by an excitation applied to the metallic IDT shown in the computational domain in Figure 8. The crystal cut is chosen as 128 X-cut Y propagating lithium niobate. The main excitation type is of Rayleigh type, however some bulk waves are also excited. These excitations if not removed appear as computational noise in the output port. Figure 16 shows the effective removal of the bulk wave type reflections by the implemented PML.

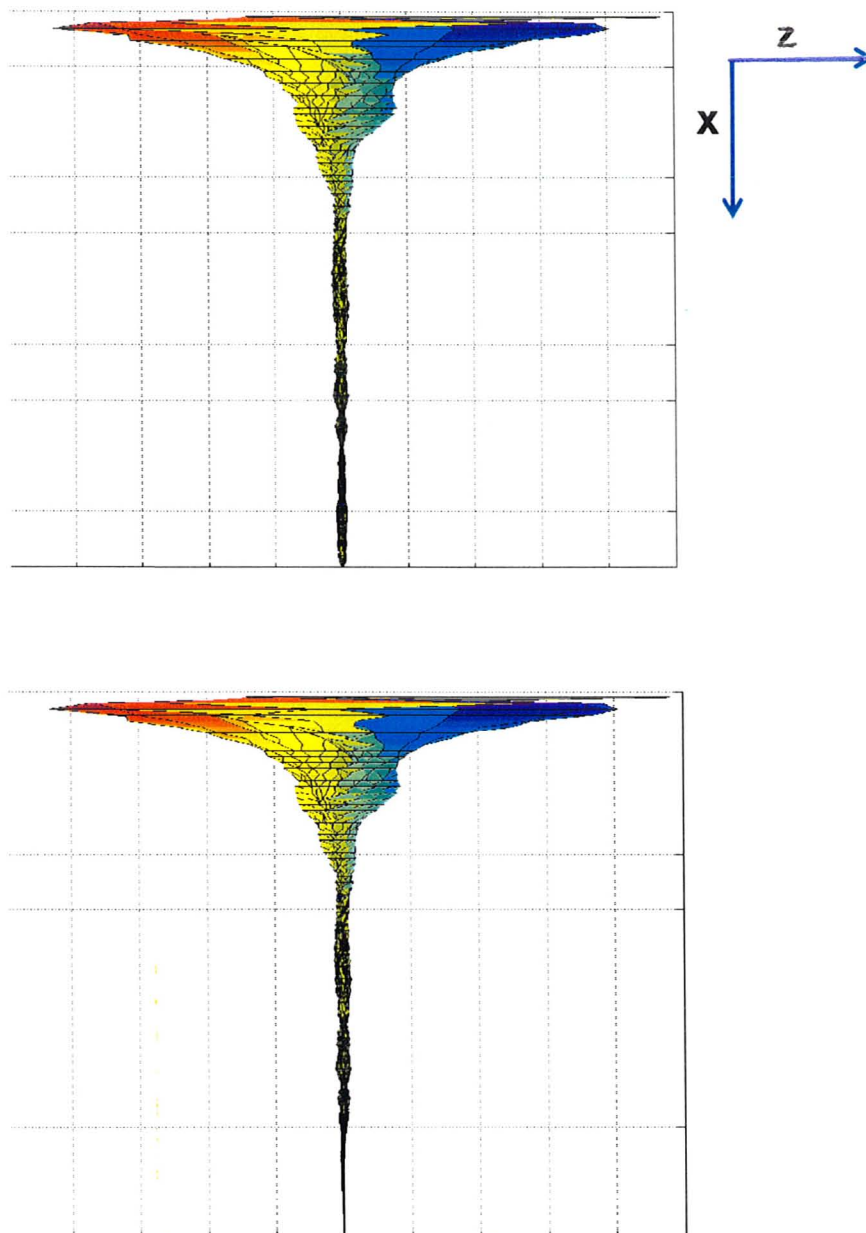


Figure 16 Absorption of the Parasitic Waves by the PML. Top: Parasitic Waves Before Introduction of the PML. Bottom: Removal of the Parasitic Waves using the PML.

Chapter 5: Conclusions

A PML for acoustic waves is developed which addressed the instability issues previously reported in [10].

A parallel derivation of the elastodynamic PML for FDTD is drawn following Bérenger's development of the electromagnetic PML. It was shown that in addition to the scalar loss-coefficients introduced for the velocity field, a loss-coefficient tensor was also necessary for the stress field components. These two loss-coefficients were shown to be connected through a matching condition that bears close resemblance to the one developed for electromagnetic waves. This condition when implemented in the FDTD time update equations of the PML, simplifies the matrix algebra to scalar math and therefore obviates the need for matrix inversion.

The results show stability under various test cases including different piezoelectric crystals and excitations. The implemented PML was then used to terminate a model of a periodic SAW device suppressing parasitic bulk wave radiation.

References

- [1] R. M. White, and F. W. Voltmer, “Direct piezoelectric coupling to surface elastic waves,” *Appl. Phys. Lett.* vol. 7, pp. 314–316, 1965
- [2] Lord Rayleigh, “On Waves Propagated along the Plane Surface of an Elastic Solid,” *Proc. London Math. Soc.* s1-17, pp. 4-11, 1885
- [3] C. K. Campbell, “Surface Acoustic Wave Devices for Mobile and Wireless Communications,” Academic Press, New York, 1998
- [4] J. Curie, and P. Curie, “Développement par pression, de l’électricité polaire dans les cristaux hémihédres à faces inclinées,” *Comptes Rendus*, vol. 91, pp. 294, 1880
- [5] B.A. Auld, *Acoustic Fields and Waves in Solids*, vol. 1, 2nd ed., New York, Kruger Publishing Co., 1990
- [6] G. Lippman, “Principe de la conservation de l’électricité,” *Annales de chimie et de physique*, vol. 24, 145, 1881
- [7] B.A. Auld, *Acoustic Fields and Waves in Solids*, vol. 2, 1st ed., New York, John Wiley & Sons, Inc., 1973
- [8] Y. Ebata, “Suppression of bulk-scattering loss in SAW resonator with quasi-constant acoustic reflection periodicity,” in *Proc. 1988 Ultrasonics Symposium*, pp. 91–96, 1988
- [9] W. Wang, et. al., “Minimizing the bulk scattering loss in CRF(DMS) devices,” in *Proc. 2004 IEEE Ultrasonics Symposium*, pp. 1363–1366, 2004
- [10] F. Chagla, and P. M. Smith, “Finite Difference Time Domain Methods for Piezoelectric Crystals,” *IEEE Transactions on Ultrasonics, Ferroelectrics, and Frequency Control*, vol. 53, no. 10, 2006
- [11] K. Bløtekjær, et. al., “A method for analyzing waves in structures consisting of metal strips on dispersive media,” *IEEE Trans. Electron. Devices*, vol. 20, pp. 1133–1138, 1973

- [12] K. Bløtekjær, et. al., “Acoustic surface waves in piezoelectric materials with periodic metal strips on the surface,” *IEEE Trans. Electron. Devices*, vol. 20, pp. 1139–1146, 1973
- [13] Y. Zhang, et. al., “Characteristic parameters of surface acoustic waves in a periodic metal grating on a piezoelectric substrate,” *IEEE Trans. Ultrason., Ferroelect. Freq. Cont.*, vol. 40, 183-192, 1993
- [14] J. Koskela, “Analysis and Modeling of Surface-Acoustic Wave Resonators,” Helsinki University of Technology Publications in Engineering Physics, 2000
- [15] M. Buchner, et. al., “FEM analysis of the reflection coefficient of SAWs in an infinite periodic array,” in *Proc. IEEE Ultrasonics Symposium*, 1991
- [16] U. Rösler, et. al., “Determination of leaky SAW propagation, reflection, and coupling on LiTaO₃,” in *Proc. IEEE Ultrasonics Symposium*, 1995
- [17] T. Sato, and H. Abe, “Propagation of longitudinal leaky surface waves under periodic metal grating structure on lithium tetraborate,” *IEEE Trans. Ultrason., Ferroelec., Freq. Cont.*, vol. 45. 304-408, 1998
- [18] R.F. Milsom, et. al., “Analysis of generation and detection of surface acoustic waves by interdigital transducers,” *IEEE Trans. Sonic. Ultrason.*, vol. 24, 147-166, 1977
- [19] C. Wang, and D. Chen, “Analysis of surface excitation of elastic wave field in a half space of piezoelectric crystal generation formulae of surface excitation of elastic field,” *Chinese J. of Acoustics*, vol. 4, pp. 232-243, 1985
- [20] A. R. Baghai-Wadji, et. al., “Green’s function applications in SAW devices,” in *Proc. IEEE Ultrason. Symp.*, pp.11-20, 1991
- [21] P. Ventura, et. al., “A mixed FEM/Analytical model of the electrode mechanical perturbations for SAW and PSAW propagation,” in *Proc. IEEE Ultrason. Symp.*, pp. 205-208, 1993
- [22] P. Ventura, et. al., “A new efficient combined FEM and periodic Green’s function formalism for the analysis of periodic SAW structures,” in *Proc. IEEE Ultrason. Symp.*, pp. 263-268, 1995

- [23] P. Ventura, and J.M. Hode, “A new accurate analysis of periodic IDTs built on unconventional orientation on quartz,” in *Proc. IEEE Ultrason. Symp.*, pp. 139-142, 1997
- [24] K. Hashimoto, and M. Yamaguchi, “Precise simulation of surface transverse wave devices by discrete Green function theory,” in *Proc. IEEE Ultrason. Symp.*, pp. 253-258, 1994
- [25] K. Hashimoto, et. al., “Coupling-of-modes modeling for fast and precise simulation of leaky surface acoustic wave devices,” in *Proc. IEEE Ultrason. Symp.*, pp. 251-256, 1995
- [26] K. Hashimoto, and M. Yamaguchi, “General-purpose simulator for leaky surface acoustic wave devices based on coupling-of-modes theory,” in *Proc. IEEE Ultrason. Symp.*, pp. 117-122, 1996
- [27] R.C. Peach, “A general Green function analysis for SAW devices,” in *Proc. IEEE Ultrason. Symp.*, pp. 221-225, 1995
- [28] V. P. Plessky, and T. Thorvaldsson, “Periodic Green’s function analysis of SAW and leaky SAW propagation in a periodic system of electrodes on piezoelectric crystal,” in *Proc. , IEEE Trans. Sonic. Ultrason. Ferroelec. Freq. contr.*, vol. 42, pp. 280-293, 1995
- [29] A. Isobe, et. al., “Propagation characteristics of longitudinal leaky SAW in Al-grating structure,” *IEEE Trans. Sonic. Ultrason. Ferroelec. Freq. contr.*, vol. 46, pp. 849-855, 1999
- [30] K.Y. Wong, and W.Y. Tam, “Analysis of the frequency response of SAW filters using finite-difference time-domain method,” *IEEE Trans. on Microwave Theory and Techniques*, vol. 53, no. 11, 2005
- [31] K.S. Yee, “Numerical solution of initial boundary value problems involving Maxwell’s equations in isotropic media,” *IEEE Trans. Antennas Propagat.*, vol. 14, pp. 302–307, 1966
- [32] A. Taflove, and S.C. Hagness, “Computational Electrodynamics: The Finite-Difference Time-Domain Method,” 2nd ed. Norwood, MA: Artech House, 2000

- [33] J.P. Bérenger, “A Perfectly Matched Layer for the Absorption of Electromagnetic Waves,” *J. of Computational Physics*, vol. 114, Issue 2, pp. 185-200, 1994
- [34] W.C. Chew, and Q.H. Liu, “Perfectly Matched Layers for Elastodynamics: A New Absorbing Boundary Condition,” *J. of Comp. Acoust.*, vol. 4, no. 4, pp. 341-360, 1996
- [35] A. Montazeri, et. al, “An approximate boundary condition for piezoelectric crystals using FDTD,” 2010 ACES Conference, The Applied computational and Electromagnetics Society, Tampere, Finland, April, 2010
- [36] J.P. Bérenger, Perfectly Matched Layer (PML) for Computational Electromagnetics, 1st ed., Morgan & Claypool, 2007

Appendix A

Symmetry Characteristics: Compliance and Stiffness Matrices

Triclinic System

21 constants

$$\begin{bmatrix}
 s_{11} & s_{12} & s_{13} & s_{14} & s_{15} & s_{16} \\
 s_{12} & s_{22} & s_{23} & s_{24} & s_{25} & s_{26} \\
 s_{13} & s_{23} & s_{33} & s_{34} & s_{35} & s_{36} \\
 s_{14} & s_{24} & s_{34} & s_{44} & s_{45} & s_{46} \\
 s_{15} & s_{25} & s_{35} & s_{45} & s_{55} & s_{56} \\
 s_{16} & s_{26} & s_{36} & s_{46} & s_{56} & s_{66}
 \end{bmatrix}$$

Monoclinic System

13 constants

$$\begin{bmatrix}
 s_{11} & s_{12} & s_{13} & 0 & s_{15} & 0 \\
 s_{12} & s_{22} & s_{23} & 0 & s_{25} & 0 \\
 s_{12} & s_{23} & s_{33} & 0 & s_{35} & 0 \\
 0 & 0 & 0 & s_{44} & 0 & s_{46} \\
 s_{15} & s_{25} & s_{35} & 0 & s_{55} & 0 \\
 0 & 0 & 0 & s_{46} & 0 & s_{66}
 \end{bmatrix}$$

Orthorhombic System

9 constants

$$\begin{bmatrix} s_{11} & s_{12} & s_{13} & 0 & 0 & 0 \\ s_{12} & s_{22} & s_{23} & 0 & 0 & 0 \\ s_{13} & s_{23} & s_{33} & 0 & 0 & 0 \\ 0 & 0 & 0 & s_{44} & 0 & 0 \\ 0 & 0 & 0 & 0 & s_{55} & 0 \\ 0 & 0 & 0 & 0 & 0 & s_{66} \end{bmatrix}$$

Tetragonal System

Classes $4, \bar{4}, 4/m$

7 constants

$$\begin{bmatrix} s_{11} & s_{12} & s_{13} & 0 & 0 & s_{16} \\ s_{12} & s_{11} & s_{13} & 0 & 0 & -s_{16} \\ s_{13} & s_{13} & s_{33} & 0 & 0 & 0 \\ 0 & 0 & 0 & s_{44} & 0 & 0 \\ 0 & 0 & 0 & 0 & s_{44} & 0 \\ s_{16} & -s_{16} & 0 & 0 & 0 & s_{66} \end{bmatrix}$$

Tetragonal System

Classes $4mm, 422,$
 $\bar{4}2m, 4/mmm$

6 constants

$$\begin{bmatrix} s_{11} & s_{12} & s_{13} & 0 & 0 & 0 \\ s_{12} & s_{11} & s_{13} & 0 & 0 & 0 \\ s_{13} & s_{13} & s_{33} & 0 & 0 & 0 \\ 0 & 0 & 0 & s_{44} & 0 & 0 \\ 0 & 0 & 0 & 0 & s_{44} & 0 \\ 0 & 0 & 0 & 0 & 0 & s_{66} \end{bmatrix}$$

Trigonal System

Classes $3, \bar{3}$

7 constants

$$\begin{bmatrix} s_{11} & s_{12} & s_{13} & s_{14} & -s_{25} & 0 \\ s_{12} & s_{11} & s_{13} & -s_{14} & s_{25} & 0 \\ s_{13} & s_{13} & s_{33} & 0 & 0 & 0 \\ s_{14} & -s_{14} & 0 & s_{44} & 0 & 2s_{25} \\ -s_{25} & s_{25} & 0 & 0 & s_{44} & 2s_{14} \\ 0 & 0 & 0 & 2s_{25} & 2s_{14} & 2(s_{11} - s_{12}) \end{bmatrix}$$

Trigonal System

$32, 3m, \bar{3}m$

6 constants

$$\begin{bmatrix} s_{11} & s_{12} & s_{13} & s_{14} & 0 & 0 \\ s_{12} & s_{11} & s_{13} & -s_{14} & 0 & 0 \\ s_{13} & s_{13} & s_{33} & 0 & 0 & 0 \\ s_{14} & -s_{14} & 0 & s_{44} & 0 & 0 \\ 0 & 0 & 0 & 0 & s_{44} & 2s_{14} \\ 0 & 0 & 0 & 0 & 2s_{14} & 2(s_{11} - s_{12}) \end{bmatrix}$$

Hexagonal System:

5 constants

$$\begin{bmatrix} s_{11} & s_{12} & s_{13} & 0 & 0 & 0 \\ s_{12} & s_{11} & s_{13} & 0 & 0 & 0 \\ s_{13} & s_{13} & s_{33} & 0 & 0 & 0 \\ 0 & 0 & 0 & s_{44} & 0 & 0 \\ 0 & 0 & 0 & 0 & s_{44} & 0 \\ 0 & 0 & 0 & 0 & 0 & 2(s_{11} - s_{12}) \end{bmatrix}$$

Cubic System:

3 constants

$$\begin{bmatrix} s_{11} & s_{12} & s_{12} & 0 & 0 & 0 \\ s_{12} & s_{11} & s_{12} & 0 & 0 & 0 \\ s_{12} & s_{12} & s_{11} & 0 & 0 & 0 \\ 0 & 0 & 0 & s_{44} & 0 & 0 \\ 0 & 0 & 0 & 0 & s_{44} & 0 \\ 0 & 0 & 0 & 0 & 0 & s_{44} \end{bmatrix}$$

Isotropic System:

2 constants

$$\begin{bmatrix} s_{11} & s_{12} & s_{12} & 0 & 0 & 0 \\ s_{12} & s_{11} & s_{12} & 0 & 0 & 0 \\ s_{12} & s_{12} & s_{11} & 0 & 0 & 0 \\ 0 & 0 & 0 & s_{44} & 0 & 0 \\ 0 & 0 & 0 & 0 & s_{44} & 0 \\ 0 & 0 & 0 & 0 & 0 & s_{44} \end{bmatrix}$$